iScience

Article

Porphyran from discolored nori prevents metabolic syndrome through microbiota-bile acid-ceramide pathway

Graphical abstract

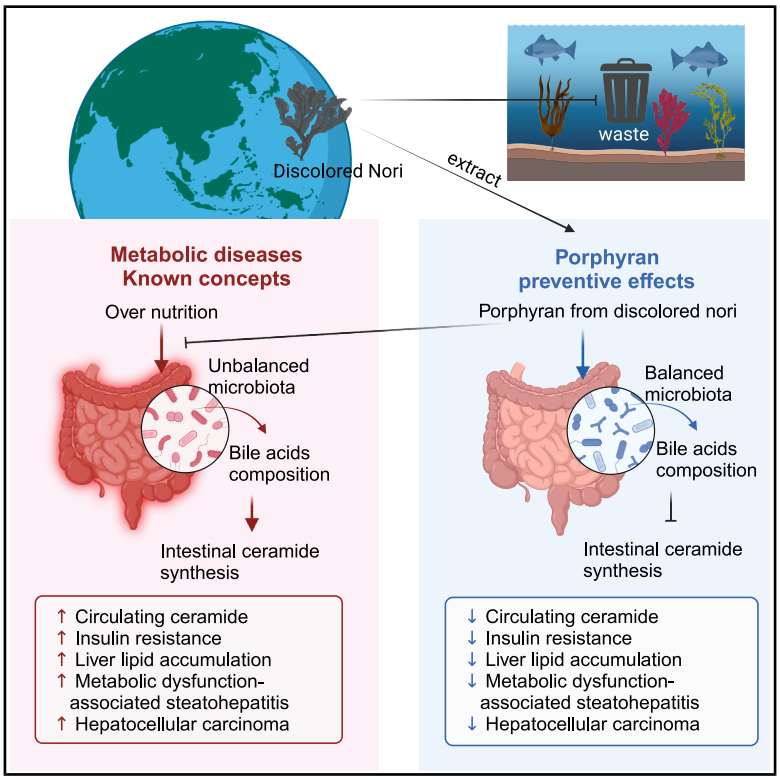

Highlights

- Porphyran is in nori, a staple food in Japan with a low rate of obesity globally
- Porphyran had disease-preventive effects in *in vivo* models of MetS, MASH, and HCC
- Porphyran may prevent disease via the gut microbiota-bile acid-ceramide pathway
- Porphyran from discolored nori can contribute to global environmental sustainability

Authors

Yoko Yokoyama, Yoko Takashina, Jean-David Morel, ..., Kazuo Tsubota, Johan Auwerx, Mitsuhiro Watanabe

Correspondence

wmitsulab@gmail.com (Y.Y.), wmitsu@keio.jp (M.W.)

In brief

Natural sciences; Biological sciences; Physiology; Endocrinology

Yokoyama et al., 2025, iScience *28*, 112603
June 20, 2025
https://doi.org/10.1016/j.isci.2025.112603

CellPress

iScience

CellPress
OPEN ACCESS

Article

Porphyran from discolored nori prevents metabolic syndrome through microbiota-bile acid-ceramide pathway

Yoko Yokoyama,[1,2,3,*] Yoko Takashina,[2] Jean-David Morel,[4] Tanon Taworntawat,[1,2] Naho Kitamura,[1,2] Utana Nagano,[2] Tatsuya Tanigaki,[2] Anna Nakamura,[2] Teruo Miyazaki,[5] Hiroki Taoka,[2] Adrienne Mottis,[4] Alessia Perino,[6] Atsushi Shinjo,[1,2] Norihiro Suzuki,[3] Setsuo Takekawa,[3] Shinji Fukuda,[1,7,8,9,10] Akira Honda,[5,11] Kenji Ishihara,[12] Makoto Arita,[13,14] Kazuo Tsubota,[2,15,16] Johan Auwerx,[4] and Mitsuhiro Watanabe[1,2,3,17,18,19,*]

[1]Graduate School of Media and Governance, Keio University, 5322, Endo, Fujisawa, Kanagawa 252-0882, Japan
[2]Health Science Laboratory, Keio Research Institute at SFC, Keio University, 5322, Endo, Fujisawa, Kanagawa 252-0882, Japan
[3]Health Science Lab Laboratories, Shonan Keiiku Hospital, 4360 Endo, Fujisawa, Kanagawa 252-0816, Japan
[4]Laboratory of Integrative Systems Physiology, Institute of Bioengineering, Ecole Polytechnique Fédérale de Lausanne, 1015 Lausanne, Switzerland
[5]Joint Research Center, Tokyo Medical University Ibaraki Medical Center, Ibaraki 300-0395, Japan
[6]Laboratory of Metabolic Signaling, Institute of Bioengineering, Ecole Polytechnique Fédérale de Lausanne, 1015 Lausanne, Switzerland
[7]Institute for Advanced Biosciences, Keio University, Tsuruoka, Yamagata 997-0052, Japan
[8]Gut Environmental Design Group, Kanagawa Institute of Industrial Science and Technology, Kawasaki, Kanagawa 210-0821, Japan
[9]Transborder Medical Research Center, University of Tsukuba, Tsukuba, Ibaraki 305-8575, Japan
[10]Laboratory for Regenerative Microbiology, Juntendo University Graduate School of Medicine, Hongo, Tokyo 113-8421, Japan
[11]Department of Gastroenterology and Hepatology, Tokyo Medical University Ibaraki Medical Center, Ibaraki 300-0395, Japan
[12]Seafood Safety and Technology Division, Fisheries Technology Institute, Japan Fisheries Research and Education Agency, Yokohama 236-8648 Japan
[13]RIKEN Center for Integrative Medical Sciences, Suehiro-cho, Tsurumi-ku, Yokohama, Kanagawa 230-0045, Japan
[14]Division of Physiological Chemistry and Metabolism, Graduate School of Pharmaceutical Sciences, Keio University, Shibakoen, Minato-ku, Tokyo 105-0011, Japan
[15]Department of Ophthalmology, Keio University School of Medicine, 35 Shinanomachi, Shinjuku-ku, Tokyo 160-8582, Japan
[16]Tsubota Laboratory, Inc., 35 Shinanomachi, CRIK E7, Shinjuku-ku, Tokyo 160-8582, Japan
[17]Faculty of Environment and Information Studies, Keio University, 5322, Endo, Fujisawa, Kanagawa 252-0882, Japan
[18]Department of Internal Medicine, Keio University School of Medicine, 35 Shinanomachi, Shinjuku-ku, Tokyo 160-8582, Japan
[19]Lead contact
*Correspondence: wmitsulab@gmail.com (Y.Y.), wmitsu@keio.jp (M.W.)
https://doi.org/10.1016/j.isci.2025.112603

SUMMARY

Nori is a component of the traditional Japanese diet. The Japanese have a low prevalence of obesity and cardiovascular disease worldwide, and components of nori may have disease-preventive effects. Here, we focused on porphyran, which is abundant in nori that is discarded due to discoloration, and investigated the effects of nori-derived porphyran on gut microbiota, bile acid composition, and ceramide synthesis. Administration of porphyran to mice prevented obesity, diabetes, metabolic dysfunction-associated steatohepatitis (MASH), and hepatocellular carcinoma (HCC). This improvement correlates with a decrease in secondary bile acids, a decrease in intestinal farnesoid X receptor (FXR) signaling, and a marked decrease in blood ceramide. Porphyran, abundant in discolored nori, should be the subject of future translational research to prevent diseases with significant unmet medical needs and improve global environmental sustainability.

INTRODUCTION

With the global increase in the prevalence of metabolic syndrome (MetS), metabolic dysfunction-associated steatotic liver disease (MASLD) has become the most common liver disease worldwide.[1] In addition, MASLD is becoming increasingly important in the etiology of hepatocellular carcinoma (HCC).[2] Despite this, definitive therapeutic procedures for these conditions have not been established, representing a significant unmet need.[3,4]

Japan has one of the lowest obesity prevalence rates in the world,[5] and its population is characterized by remarkable longevity.[6] A modeling analysis involving eight countries using data on the prevalence of obesity and diabetes found that Japan had the most conservative estimated increase in the rate of progression of MASLD, particularly metabolic

dysfunction-associated steatohepatitis (MASH).[7] Given the important role of dietary factors in noncommunicable disease-related mortality,[8,9] much research has focused on the potential of traditional Japanese diets.[10] Seaweed is a component of the Japanese traditional diet, and its potential role in health promotion is increasingly highlighted.[11] In particular, nori is a major seaweed in the Japanese diet and is still frequently consumed by Japanese, for example in sushi and onigiri (rice balls wrapped in nori). The richest biologically active compound in nori is the sulfated polysaccharide porphyran.[12] Recent studies have shown that discarded discolored nori contains higher amounts of porphyran than normal market-quality nori.[13] Extraction of porphyran from discarded discolored nori would offer dual benefits: potential applications in disease prevention and enhanced sustainability of the food supply system. Previous studies on the health-promoting effects of porphyran have shown efficacy in improving MetS and related symptoms.[12–14] However, the molecular mechanism of these effects remains to be elucidated.

Porphyran is a soluble fiber, which is assumed to alter the gut microbiota. We have focused our research on disease prevention mechanisms involving the gut microbiota. Metabolites of the gut microbiota have attracted interest as potentially explaining the black box between gut microbiota and disease prevention. Bile acids (BAs) are produced by the liver and transformed into secondary BA by the gut microbiota in the intestine. Secondary BAs are present at several millimolar concentrations in the intestine and are re-absorbed at high concentrations in the blood.[15] Both primary and secondary BAs regulate triglyceride (TG), cholesterol, energy, and glucose homeostasis through the activation of diverse signaling pathways, such as farnesoid X receptor (FXR)[16] and TGR5.[17] Thus, BA-regulated signaling pathways are promising novel drug targets for treating common metabolic diseases[18–21] such as obesity, type 2 diabetes, and hyperlipidemia; for example, BA-adsorbing resins (BABRs) were approved by the Food and Drug Administration in 2008 for the treatment of diabetes.[22,23]

In previous studies, long-term administration of the synthetic FXR agonist GW4064 induced adverse effects such as decreased basal metabolic rate, weight gain, and hepatic lipid accumulation.[24] Conversely, administration of BABR, which promotes BA efflux in the intestine, prevented hepatic lipid accumulation.[23] In this case, fibroblast growth factor 15 (FGF15) is an endocrine peptide expressed specifically in the intestine. Expression is induced by the BA-FXR pathway[25] and is upregulated by long-term treatment with GW4064[24] but downregulated by treatment with BABR.[23,26] This suggests that the presence or absence of FXR pathway activity in the intestine has some effect on lipid metabolism in the liver.

On the other hand, the intestine-specific FXR agonist fexaramine altered BA composition[27] and increased lithocholic acid (LCA),[27] a strong agonist of TGR5.[28] This in turn activated the intestinal TGR5 pathway, which led to increased glucagon-like peptide-1 (GLP-1) secretion in the intestine[29] and enhanced thermogenesis in brown adipose tissue (BAT).[17] These effects contributed to the amelioration of metabolic abnormalities.[27,30] These results demonstrate the importance of BA composition metabolized by the gut microbiota as well as the presence of FXR pathway activity in the intestine.

Recent discoveries have revealed that intestinal FXR regulates a number of genes responsible for intestinal ceramide synthesis.[31,32] Ceramides promote fatty acid synthesis via the sterol regulatory element-binding protein-1 pathway in hepatocytes by enhancing fatty acid uptake,[33] impairing β-oxidation and respiration in mitochondria,[34] and promoting lipid accumulation in the liver.[32] Increases in specific BAs, such as tauro-β-muricholic acid (TβMCA) and glycine-β-muricholic acid, which inhibit intestinal FXR,[32,35] have shown therapeutic effects on MASLD[32] and MASH[35] *in vivo*. In particular, long-term treatment with the synthetic FXR agonist GW4064 resulted in up-regulation of gene expression related to ceramide synthesis in the gut.[36] These results are consistent with our previous results showing that treatment with GW4064 activates FXR, thereby causing obesity, diabetes, and fatty liver,[24] and conversely, that BABR administration reduces FXR activity and ameliorates obesity, diabetes, and fatty liver.[23] These results suggest that the FXR-ceramide pathway may be involved in the mechanism of our earlier findings.

Porphyran content is particularly high in discarded discolored nori. This compound, a sulfated polysaccharide, is thought to act as a substrate for gut microbiota and may have the ability to shift the gut microbiota. This putative effect is in turn expected to alter the composition of BAs metabolized by the gut microbiota and thereby affect FXR signaling in the intestine. The primary aim of our present research is to investigate the preventive efficacy of porphyran extracted from discarded discolored nori, a form of food waste, against MetS and MASLD-MASH-HCC. Here, we clarify the biological mechanism of the preventive effect of porphyran extracted from seaweed waste on the gut microbiota-BA-ceramide pathway and propose a new strategy for approaching MetS using functional substances extracted from food waste.

RESULTS

Porphyran extracted from discarded discolored nori protects against features of high-fat diet-induced MetS

To evaluate the metabolic effects of an extract of nori and its bioactive compound porphyran (Figure 1A),[37] we fed 6-week-old C57BL/6J male mice a chow diet (CD; 10% kcal fat), a high-fat diet (HFD; 60% kcal fat), a porphyran-supplemented HFD (HFD-P; 60% kcal fat with 2% w/w porphyran), or an HFD supplemented with nori extract (multiple polysaccharide complexes) (HFD-Ex; 60% kcal fat with 2% w/w nori extract) for 13 weeks. The porphyran and nori extracts were obtained from discarded discolored nori.

HFD-fed mice gained weight quickly, but this effect was significantly attenuated by supplementation with porphyran or nori extract (Figure 1B). Total food intake was similar across the HFD, HFD-P, and HFD-Ex groups (Figure 1C). At the end of the study, the weight of the liver and mesenteric white adipose tissue (mWAT) in the HFD-P or HFD-Ex animals was decreased compared to HFD (Figures 1D and 1E). Mesenteric adipose tissue, which drains into the portal vein and supplies metabolites such as free fatty acids to the liver, is considered the most representative analog of human visceral fat.[38] The analysis of fat in this study accordingly focused on mesenteric adipose tissue.

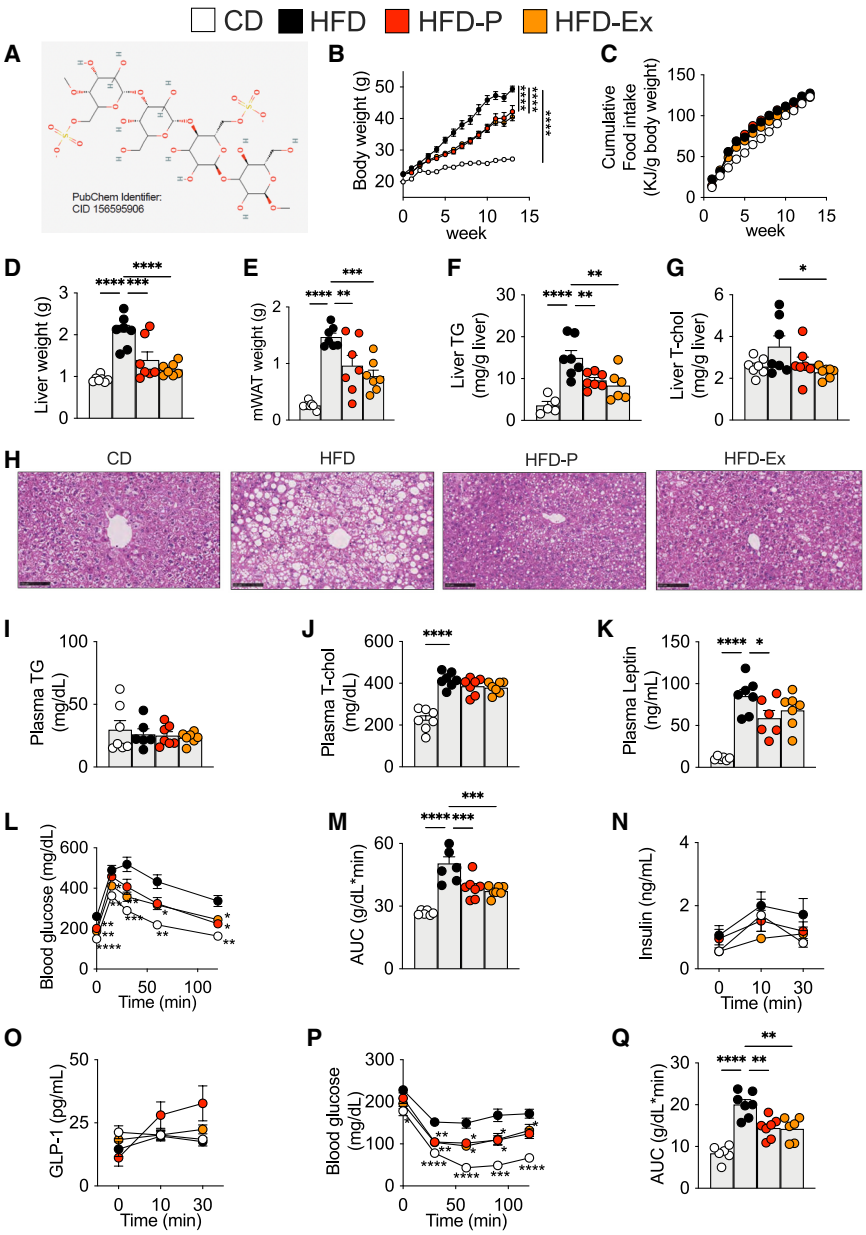

Figure 1. Porphyran and nori extracts protect against features of the high-fat diet-induced metabolic syndrome

(A) Chemical structure of porphyran (PubChem Identifier, CID 163304497).[37]

(B) Change of body weight across the different groups.

(C) Cumulative food intake per body weight.

(D) Liver tissue weight.

(E) Mesenteric adipose tissue (mWAT) weight.

(F and G) Liver triglycerides (TG) (F) and total cholesterol (T-chol) (G).

(H) Representative sections of liver tissue stained with hematoxylin and eosin (H&E). Scale bars, 100 μm.

(I–K), Plasma TG (I), total cholesterol (J), and leptin (K) levels.

(L) Oral glucose tolerance test (OGTT) after an overnight fast, 10 weeks after initiation of dietary treatment. Glucose was administered by gavage at a dose of 1.5 g/kg body weight. Comparison to HFD.

(M) Area under the curve (AUC) of the glucose excursion during the OGTT in (L).

(N) Plasma insulin levels during the first half hour of the OGTT.

(O) Plasma glucagon-like peptide-1 (GLP-1) levels during the first half hour of the OGTT.

(P) Intraperitoneal insulin tolerance test (IPITT) after 11 weeks of treatment, after a 4 h fast. Insulin was injected at dose of 0.75 U/kg body weight. Comparison to HFD.

(Q) AUC of glucose levels during IPITT. CD, control diet; HFD, high-fat diet; HFD-P, high-fat diet with porphyran; HFD-Ex, high-fat diet with nori extract. n = 7/animals/group.

Data are represented as mean ± SEM. $^{*}p < 0.05$, $^{**}p < 0.01$, $^{***}p < 0.001$, $^{****}p < 0.0001$, comparison to HFD. p values calculated using analysis of variance, assessed by Holm-Šídák's multiple comparisons test. See also Figure S1.

Hepatic TG levels were increased upon HFD feeding. However, this effect was attenuated by HFD-P and HFD-Ex diets (Figure 1F). Furthermore, analysis of liver lipid profiles revealed a significant reduction in hepatic total cholesterol in HFD-Ex mice compared to HFD mice and a tendency toward a reduction in hepatic total cholesterol in the HFD-P group (Figure 1G). Representative images of liver sections stained with hematoxylin and eosin showed that HFD induced fat accumulation, which was reduced in the HFD-P and HFD-Ex groups (Figures 1H and S1). Plasma TG levels were not changed across the different diets (Figure 1I). In contrast, plasma total cholesterol was increased in the HFD group but was not decreased in the HFD-P or HFD-Ex groups (Figure 1J). The adipocyte-derived hormone leptin was increased in the HFD group but decreased in the HFD-P group (Figure 1K).

In an oral glucose tolerance test (OGTT), the excursion of blood glucose levels was higher in HFD animals than in CD animals, while HFD-P and HFD-Ex animals showed an intermediate phenotype (Figure 1L), as also indicated by the area under the curve (Figure 1M). Plasma insulin and GLP-1 levels during OGTT did not differ between the groups, although plasma GLP-1 tended to increase in HFD-P-fed mice (Figures 1N and 1O). Similarly, in an intraperitoneal insulin tolerance test (IPITT), HFD mice showed higher blood glucose levels than CD mice, a finding which was partially reverted in the HFD-P and HFD-Ex groups (Figures 1P and 1Q).

Porphyran reverts the transcriptome-level effects of HFD across tissues

To further analyze the effect of these treatments on different metabolic organs, we conducted microarray gene analysis in

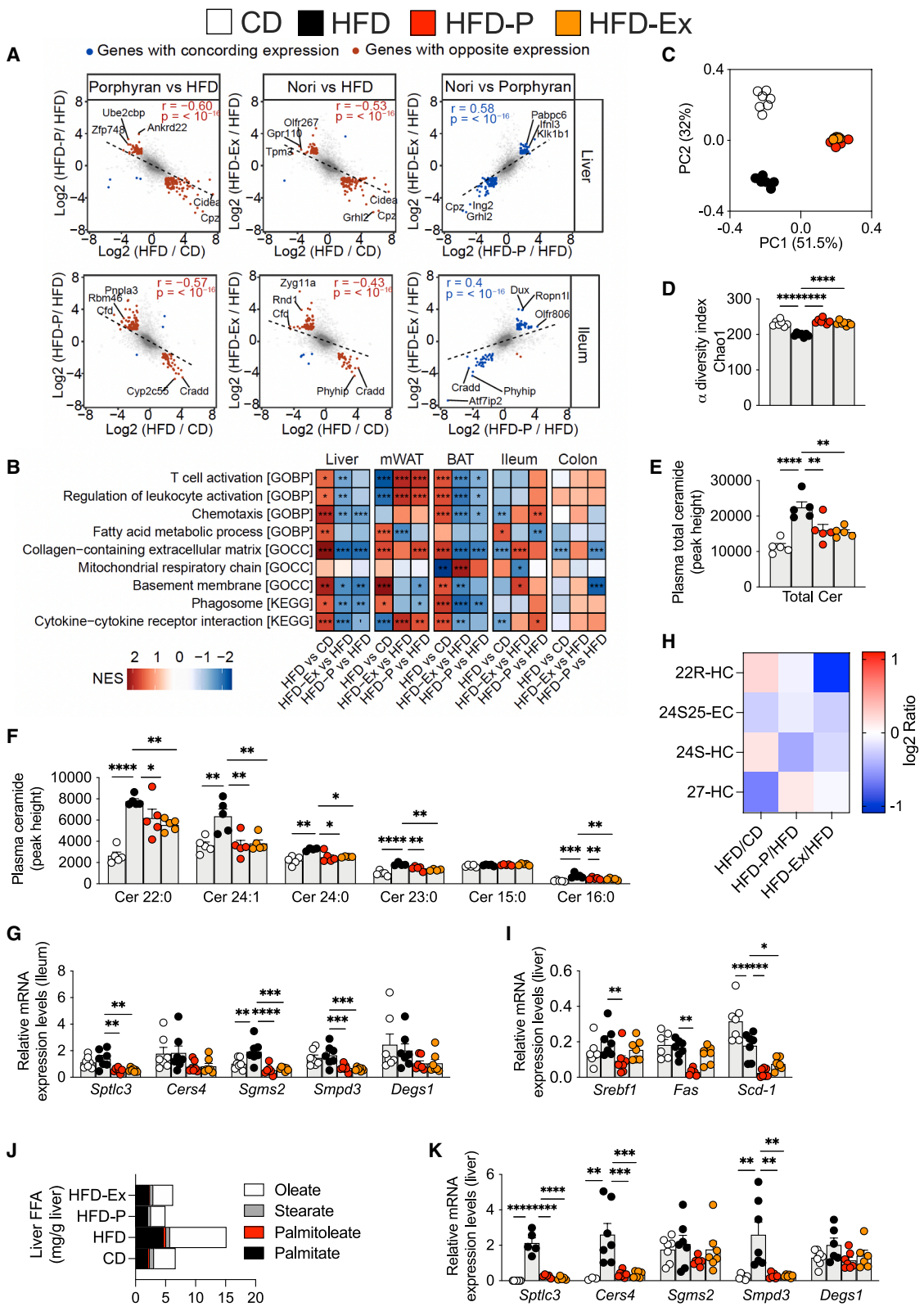

(legend on next page)

the liver, ileum, mWAT, BAT, and colon. For each organ, we compared the effect of the HFD with that of porphyran or nori extract and found a striking, transcriptome-level reversion of the effect of an HFD in every organ tested (Figures 2A and S2).

In all tissues, we observed very strong negative correlations between the effects of HFD and those of HFD-P (liver: $r = -0.60$, $p < 10^{-16}$, ileum: $r = -0.57$, $p < 10^{-16}$, mWAT: $r = -0.78$, $p < 10^{-16}$, BAT: $r = -0.50$, $p < 10^{-16}$, colon: $r = -0.40$, $p < 10^{-16}$) (Figures 2A and S2, left panels), indicating that porphyran reverts the effects of HFD at the transcriptome level. A similar reversion was observed with nori extract (Figures 2A and S2, central panels). The effects of porphyran and nori extract were robustly correlated to one another in every organ (Figures 2A and S2, right panels). This result suggests that porphyran is indeed the active compound of nori and sufficient to mediate its effects.

To get an overview of the pathways affected by porphyran or nori supplementation, we performed a gene set enrichment analysis. The full results of the analysis are displayed in Table S2. For this, we selected a few of the most differentially expressed, non-redundant gene sets (Figure 2B). Inflammation-related gene sets were increased by HFD in the liver but reversed in HFD-P or HFD-Ex mice (Figure 2B). Collagen-containing extracellular matrix components were robustly enriched by HFD in the liver, suggesting that HFD triggered liver fibrogenesis, and porphyran or nori extract was able to reverse this effect (Figures 2B and S3; Table S2). These results suggest that porphyran or nori extract may have a reversing effect on MASH, which is primarily characterized by inflammation and fibrosis.

Porphyran reshapes the gut microbiota

Nori has been previously shown to impact the gut microbiota and promote colonization by porphyran-degrading bacteria.[39] To analyze the impact of our dietary intervention on microbiome composition, we profiled the fecal microbiota using 16S rRNA gene profiling (Figures S4 and S5). Principal coordinate analysis revealed distinct clustering of the gut microbiome between microbiota from CD, HFD, and HFD-P or HFD-Ex animals (Figure 2C). Importantly, while HFD caused a loss of alpha diversity, the addition of porphyran or nori extract restored this diversity (Figure 2D).

At the phylum level, Bacteroidetes were increased and Firmicutes were decreased by HFD-P or HFD-Ex (Figure S4A). At the family level, Paraprevotellaceae were decreased by HFD compared to CD but were recovered in HFD-P or HFD-Ex animals (Figure S4B). At the genus level, *Prevotella* was significantly increased in HFD-P and HFD-Ex, and *Sutterella* was increased in HFD-P (Figure S4C). The microbial species increased by HFD were almost uniformly diminished by HFD-P or HFD-Ex. HFD-P or HFD-Ex shared patterns of gut microbiota, but these were different from both HFD and CD, indicating that porphyran or nori extract did not completely restore the gut microbiota of CD-fed mice but rather induced a new equilibrium (Figures S5A–S5E).

Porphyran lowers ceramide levels

Ceramides are considered to be bioactive lipids, and elevation of ceramide levels has been reported in diseases linked with MetS,[40–42] MASH,[35] HCC,[43] and other disorders.[44] Indeed, ceramides have recently been proposed as promising candidate biomarkers for these diseases.[45] In line with this hypothesis, while plasma ceramides were increased in our HFD-fed mice (Figures 2E and 2F), porphyran and nori extract supplementation robustly reduced total plasma ceramide levels (Figure 2E), as well as levels of each ceramide species except C15:0 (Figure 2F).

Recent studies have shown that BAs metabolized by the gut microbiota regulate FXR signaling.[32] Previous studies have shown that the hepatic FXR/small heterodimer partner pathway inhibits hepatic lipogenesis[16] but that the synthetic FXR agonist GW4064 promotes lipid accumulation in the liver.[24] These seemingly contradictory results suggest the possibility of inter-organ communication, and recent studies have focused on FXR in the intestine and enterohepatic circulation.[46] In the present study, porphyran extracted from discolored nori, a natural substance, altered the gut microbiota, causing changes in the composition of BAs while decreasing the FXR agonists chenodeoxycholic acid (CDCA), deoxycholic acid, LCA, and cholic acid, as well as the gene expression of FXR-regulated FGF15 and ileal BA-binding protein (IBABP) in the intestine (Figures S6A and S6B). The results of liver BA composition analysis also showed that free secondary BAs in the liver, which are assumed to reflect BA composition reabsorbed from the ileum, were decreased in the HFD-P and HFD-Ex groups (Figure S7A). Furthermore, *Cyp7a1* expression in the liver was significantly elevated in the HFD-P group compared to HFD (Figure S7B), suggesting that the negative feedback was

Figure 2. Porphyran or nori extract changes the composition of the gut microbiota and lipid metabolism

(A) Microarray mRNA expression analysis of liver and ileum samples. Tissues from the 7 mice in a group were pooled.

(B) Selected gene set comparisons by GOBP (Gene Ontology Biological Process), GOCC (Gene Ontology Cellular Component), and KEGG (Kyoto Encyclopedia of Genes and Genomes).

(C) Principal coordinate analysis of the 16S rRNA gene data.

(D) α diversity index (Chao1).

(E and F) Plasma total ceramides (E), each ceramide species (F). Plasma ceramides were measured 5 per group.

(G) Relative transcript levels of genes involved in ceramide synthesis pathway in the ileum.

(H) Oxysterol composition in the liver. The oxysterols were measured in pooled liver samples per treatment group ($n = 7$/group).

(I) Relative transcript levels of genes involved in fatty acid synthesis pathway in the liver.

(J) Free fatty acid (FFA) composition in liver. The FFAs were measured in pooled liver samples per treatment group ($n = 7$/group).

(K) Relative transcript levels of genes involved in ceramide synthesis pathway in the liver. CD, control diet; HFD, high-fat diet; HFD-P, high-fat diet with porphyran; HFD-Ex, high-fat diet with nori extract; mWAT, mesenteric white adipose tissue; 22R-HC, 22*R*-hydroxycholesterol; 24S25-EC, 24(S),25-epoxycholesterol, endogenous cholesterol metabolite; 24S-HC, 24*S*-hydroxycholesterol; 27-HC, 27-hydroxycholesterol. $n = 7$/animals/group.

Data are represented as mean ± SEM. $^{*}p < 0.05$, $^{**}p < 0.01$, $^{***}p < 0.001$, $^{****}p < 0.0001$. p values calculated using analysis of variance, assessed by Holm-Šídák's multiple comparisons test. See also Figures S2–S8.

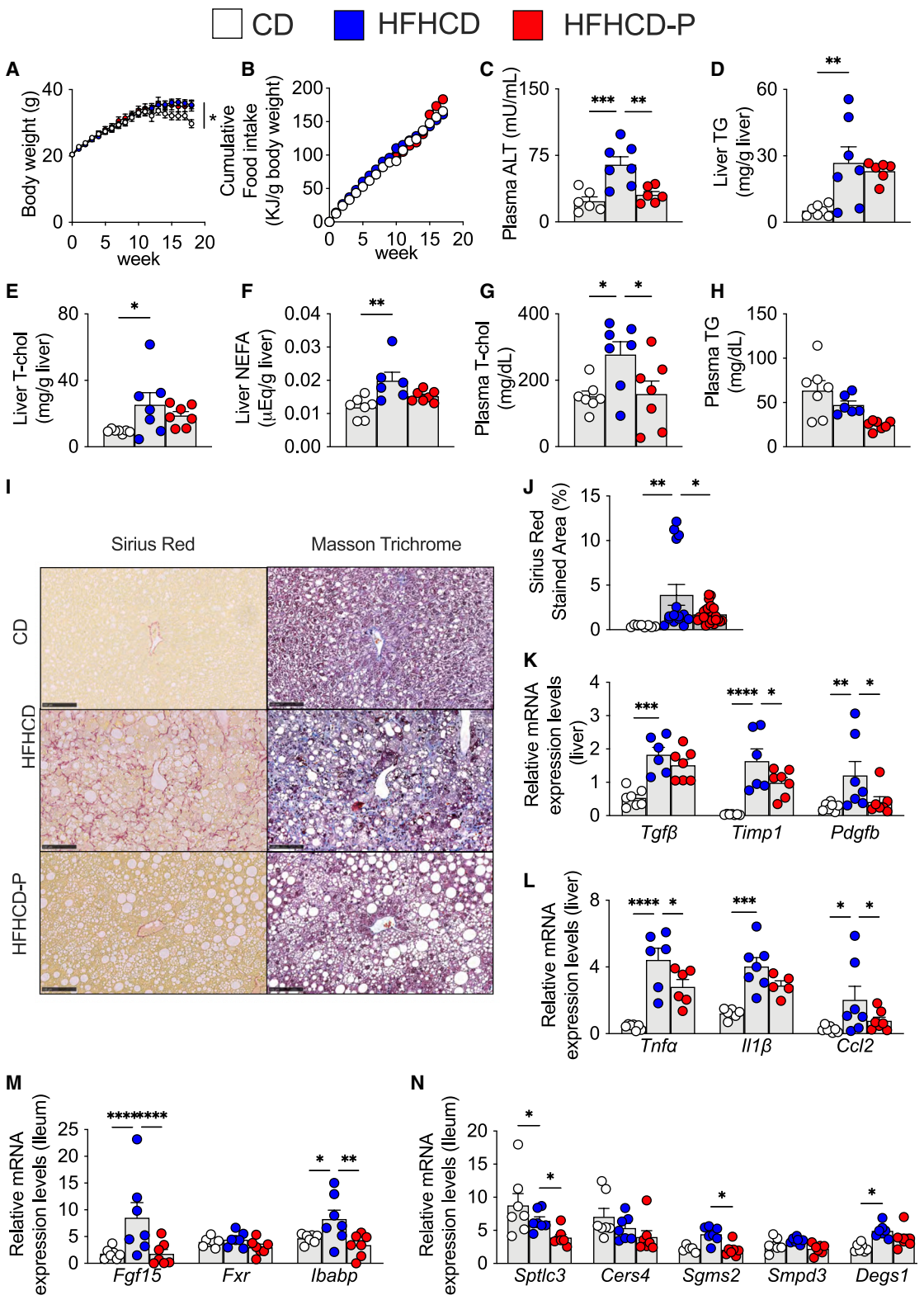

Figure 3. Porphyran prevents liver function, fibrosis, and inflammation against high-fat and high-cholesterol diet-induced MASH

(A) Change in body weight. Diet was provided from the start (week 0).

(B) Cumulative food intake per body weight.

(legend continued on next page)

reduced due to a decrease in FGF15 associated with decreased FXR signaling in the ileum. In addition, intestinal FXR regulates the expression of genes in the ceramide synthesis pathway. Indeed, transcript levels of enzymes in the sphingomyelinase-mediated ceramide synthesis pathways, *Smpd3*, as well as in the *de novo* ceramide synthesis pathway, such as *Sptlc3*, were reduced in the ileum of porphyran- or nori extract-treated mice (Figures 2G and S8).

Furthermore, since previous studies have shown that decreased intestinal ceramide synthesis is associated with suppressed fatty acid synthesis in the liver, we analyzed the composition of oxysterols, the ligands for the liver X receptor (LXR), which regulates the fatty acid synthesis pathway. Oxysterols, the oxidized forms of cholesterol, are ligands for the LXR,[16,47] which regulates fatty acid synthesis. Oxysterols, especially 22*R*-hydroxycholesterol and 24*S*-hydroxycholesterol, two key LXR ligands,[47–50] were decreased by HFD-P or HFD-Ex (Figure 2H). We confirmed by quantitative reverse-transcription PCR analysis of liver samples that the expression levels of *Srebf1*, as well as of key transcripts involved in fatty acids synthesis, *Fas* and *Scd-1*, were decreased in the HFD-P or HFD-Ex groups (Figure 2I). Consistent with this, free fatty acid levels, in particular oleate and the ceramide precursor palmitate,[51,52] increased in the liver in HFD mice but not in HFD-P and HFD-Ex mice (Figure 2J). In our study, the expression of genes from the ceramide *de novo* or salvage synthesis pathway in the liver was decreased in HFD-P and HFD-Ex mice (Figure 2K). Recently, a decrease in blood ceramides has also been linked to improvement in MetS and associated MASH and HCC,[53] which led us to investigate whether porphyran could also have ameliorative effects on these diseases.

Porphyran prevents liver function, fibrosis, and inflammation against high-fat and high-cholesterol diet-induced MASH

To evaluate the impact of porphyran in a MASH model, we fed 6-week-old C57BL/6J male mice a CD (10% kcal fat, no cholesterol), a diet high in fat and cholesterol (high-fat and high-cholesterol diet, HFHCD; 40% kcal fat and 2% w/w cholesterol—MASH model),[54,55] or an HFHCD supplemented with 2% w/w porphyran (HFHCD-P) for a period of 18 weeks. For body weight, HFHCD-fed mice were slightly heavier than CD-fed mice but similar to HFHCD-P-fed mice after 18 weeks (Figure 3A), with no difference in total food intake between HFHCD and HFHCD-P mice (Figure 3B). Porphyran supplementation decreased plasma alanine aminotransferase (ALT) levels, an indicator of liver damage, compared to the HFHCD-fed mice (Figure 3C). Liver TG, total cholesterol, and non-esterified fatty acid levels were increased by the HFHCD but were not decreased by supplementation with porphyran, although there was, in each case, a tendency toward a decrease (Figures 3D–3F). Finally, plasma total cholesterol levels were lower in HFHCD-P-fed relative to HFHCD-fed mice, whereas plasma TG only tended to decrease (Figures 3G and 3H).

Staining with Sirius red, which stains collagen-rich fibrotic fibers in red, was much more pronounced in the HFHCD-fed mice and reduced in the HFHCD-P-fed mice (Figure 3I, left panels). Similarly, Masson's trichrome, which stains collagen-rich fibrotic fibers in blue, showed intense staining in the HFHCD-fed but not the HFHCD-P-fed mice (Figure 3I, right panels). Quantification of the area stained with Sirius red confirmed that fibrotic fibers were robustly increased in HFHCD-fed mice but decreased in HFHCD-P-fed mice (Figure 3J). Furthermore, the HFHCD-fed mice had increased expression levels of fibrosis-related genes, but their expression was decreased in HFHCD-P mice, in particular for *Timp1* and *Pdgfb* (Figure 3K). In addition, inflammatory markers, such as tumor necrosis factor α (*Tnfα*) and C-C motif chemokine ligand 2 (*Ccl2*), were also decreased by porphyran (Figure 3L). In the MASH model, there was also a significant decrease in the HFHCD-P group in the intestinal FXR signaling downstream factors *Fgf 15* and *Ibabp* (Figure 3M) and significant decreases in ceramide synthesis-related genes *Sptlc3* and *Sgms2* (Figure 3N). Taken together, these results show that porphyran supplementation was sufficient to attenuate the main hallmarks of MASH, namely fibrosis and inflammation.

Porphyran prevents against a HFD with DMBA-induced HCC

Since MASH can progress to liver cirrhosis and ultimately HCC, we decided to investigate the effects of porphyran supplementation in an obesity-facilitated HCC model, in which carcinogen treatment causes liver cancer in mice fed a HFD.[56] Neonatal C57BL/6J mice were treated with the chemical carcinogen DMBA (7,12-dimethylbenz(a)anthracene), and then, from 6 weeks of age, were fed either a CD (10% kcal fat) (CD + DMBA), a HFD (60% kcal fat) (HFD + DMBA), or an HFD supplemented with 2% w/w porphyran (HFD + DMBA-P) for a total period of 31 weeks.

Body weight was higher in HFD + DMBA groups compared to the CD + DMBA mice (Figure 4A). Cumulative food intake was lower in HFD + DMBA and HFD + DMBA-P mice relative to the

(C) Plasma alanine amino transferase (ALT) levels.
(D–F) Liver triglycerides (TG) (D), total cholesterol (T-cho) (E), and non-esterified fatty acid (NEFA) (F) levels.
(G and H) Plasma T-cho (G) and TG (H) levels.
(I) Representative images of liver sections stained with Sirius red and Masson's trichrome. Scale bars, 100 μm.
(J) Sirius red-stained area (%) in the liver.
(K) Relative transcript levels of genes involved in fibrosis in the liver.
(L) Relative transcript levels of inflammation-related genes in the liver.
(M) Relative transcript levels of genes involved in FXR pathway in the ileum.
(N) Relative transcript levels of genes involved in ceramide synthesis pathway in the ileum. CD, control diet; HFHCD, high-fat and high-cholesterol diet; HFHCD-P, high-fat and high-cholesterol diet with porphyran. n = 7/animals/group.
Data are represented as mean ± SEM. *$p < 0.05$, **$p < 0.01$, ***$p < 0.001$, ****$p < 0.0001$. p values calculated using analysis of variance, assessed by Holm-Šídák's multiple comparisons test. Outliners detected by ROUT method with Prism was excluded from the analysis.

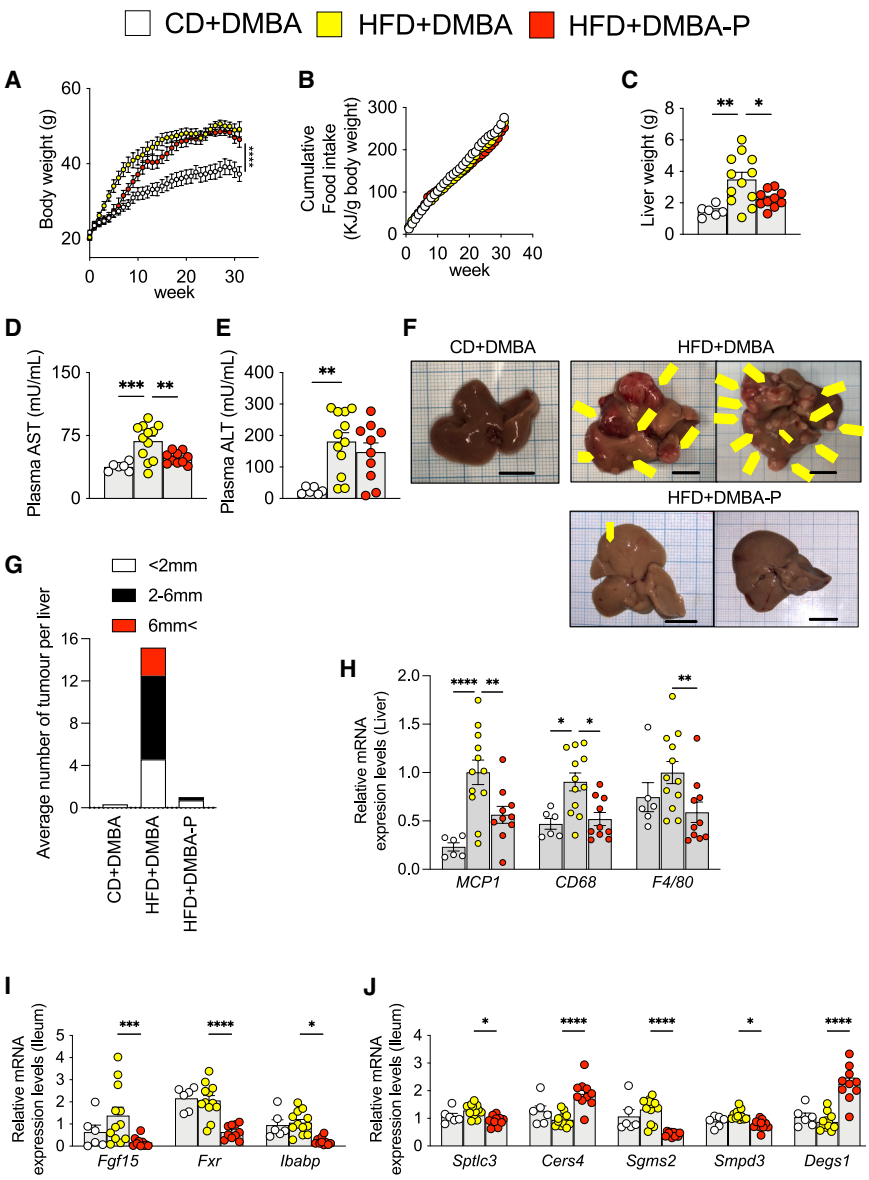

Figure 4. Porphyran prevents livers against high-fat diet with DMBA-induced HCC

(A) Change in body weight.

(B) Cumulative food intake per body weight.

(C) Liver weight.

(D) Plasma aspartate aminotransferase (AST) levels.

(E) Plasma alanine aminotransferase (ALT) levels.

(F) Representative pictures of livers. Arrowheads indicate HCCs. Scale bars, 1 cm.

(G) The average number of tumors per liver and their relative size distribution.

(H) Relative transcript levels of genes involved in inflammation in the liver.

(I) Relative transcript levels of genes involved in FXR pathway in the ileum.

(J) Relative transcript levels of genes involved in ceramide synthesis pathway in the ileum. CD + DMBA, control diet with DMBA treatment; HFD + DMBA, high-fat diet with DMBA treatment; HFD + DMBA-P, high-fat diet with DMBA treatment and with porphyran; DMBA, tumorigenic 7,12-dimethylbenz(a)anthracene. n = 6–12/animals/group. Data are represented as mean ± SEM. $^{*}p < 0.05$, $^{**}p < 0.01$, $^{***}p < 0.001$. p values calculated using analysis of variance, assessed by Holm-Šídák's multiple comparisons test. See also Figure S9.

CD + DMBA group during the test period (Figure 4B). Porphyran reduced liver weight (Figure 4C) and levels of aspartate aminotransferase, an indicator of liver damage, compared to HFD + DMBA mice (Figure 4D). Levels of ALT did not differ between the HFD + DMBA and HFD + DMBA-P groups (Figure 4E). In the HFD + DMBA group, a large number of HCCs were evident, but porphyran supplementation almost totally prevented the development of liver cancer (Figure 4F). The average numbers of large (over 6 mm), medium (2–6 mm), and small (less than 2 mm) HCCs were 2.7, 7.9, and 4.6 in HFD + DMBA mice; porphyran supplementation dramatically reduced these numbers to 0, 0.3, and 0.7 (Figure 4G). Our data hence demonstrate that porphyran supplementation is sufficient to prevent HCC. To investigate the mechanism of this HCC-preventive effect of porphyran treatment, we examined the expression of inflammation-related genes, which demonstrated upregulation in the HFD + DMBA group and downregulation in the HFD + DMBA-P group (Figure 4H). The expression of FXR downstream genes, *Fgf15* and *Ibabp*, in the intestine was significantly reduced in the HFD + DMBA-P group (Figure 4I). Additionally, the gene expression of the intestinal ceramide synthesis-related genes was also markedly diminished (Figure 4J), indicating a reduction in ceramide synthesis within the intestine in the HCC model, as observed in other models. The results of the transcriptome analysis of the liver also demonstrated that the porphyran-treated group exhibited greater decreases in cholesterol and lipid metabolism than the HCC model animals (Figure S9). This was postulated to be partly due to improvement in the abnormal lipid metabolism caused by HCC.

DISCUSSION

Porphyran and the gut microbiota-BA-ceramide pathway

In this study, the effects of porphyran extracted from discarded discolored nori on MetS, MASLD, MASH, and HCC were investigated. Our results in different mouse models suggested that porphyran treatment reduced ceramide in blood and prevented MetS, MASLD, MASH, and HCC. A possible mechanism for this effect is that the sulfated polysaccharide porphyran may alter the gut microbiota and affect BA composition, thereby modulating FXR activity. Consistent with this hypothesis,

intestinal FXR signaling was reduced, and FXR-regulated intestinal ceramide synthesis genes, as well as blood-circulating ceramides, were reduced. Previous research has demonstrated the involvement of C16:0 ceramide in obesity-related insulin resistance.[34,57] Our present study found that porphyran administration significantly reduced C16:0 ceramide levels. Further research is required to elucidate the relationship between porphyran and the enzymes responsible for synthesizing specific ceramide molecular species.

Additionally, prior studies have shown that a decrease in blood ceramide levels can activate beige fat thermogenesis,[31] which may explain the weight loss observed in the porphyran-treated group (Figure S10). Moreover, lipid synthesis in the liver was downregulated, consistent with previous studies that have demonstrated how reduced intestinal ceramide synthesis can suppress liver lipid accumulation and prevent MASLD[32] and MASH.[35] These findings suggest that the gut microbiota-BA-ceramide pathway can be effectively modulated through dietary interventions.

Porphyran administration changed the gut microbiota

Porphyran from discarded discolored nori is a natural functional substance and is found in foods consumed on a regular basis, including those in meals. It is significant that this study showed that functional substances extracted from food can prevent disease via the gut microbiota-BA-ceramide pathway. In recent years, many studies have been published on the relationship between the gut microbiota and disease.[58] Although the link between the gut microbiota and disease is still largely a black box, our present results indicate new possibilities with a dietary approach.

In the present study, porphyran derived from discarded discolored nori shifted the gut microbiome to a completely different composition and, accordingly, the fecal BA composition was also markedly different. The precise mechanism by which porphyran exerts this influence on the gut microbiota remains to be elucidated. Porphyran-induced changes in the gut microbiota were quite different from those in mice treated with HFD, with a characteristic increase in *Prevotella* and *Sutterella*. *Prevotella* has been reported to inversely correlate with MASLD[59] and MASH[60] in human studies, and although the mechanism is not clear, the fact that the gut microbiota that is remodeled and reduced in MASLD and MASH is increased by porphyran may explain the role of the gut microbiota in disease prevention.

It has been reported that Bacteroides is often increased in cases of HCC. However, it is important to note that these studies were cross-sectional in design, and thus the causal relationship between Bacteroides and HCC remains unproven.[61] Conversely, a recent study found that Bacteroides produces indole-3-acetic acid, a compound that enhances responsiveness to cancer chemotherapy.[62] Similarly, it is conceivable that the observed increase in Bacteroides in the porphyran group may exert an inhibitory effect on carcinogenesis, which could explain the increase in Bacteroides observed in this group. Furthermore, Bacteroides is capable of degrading the porphyran administered in this study.[39] Therefore, the observed increase in Bacteroides is unlikely to be a consequence of the disease itself but rather a result of its capacity to break down porphyran. Moreover, it has been shown that the gut microbiota can synthesize ceramide.[63] Consequently, future research should investigate ceramide synthesis mediated by gut microbiota.

Sutterella are known to be significantly increased in diabetic patients after Roux-en-Y gastric bypass surgery (RYGB).[64] Elevated blood BAs and decreased ceramide levels have been reported after RYGB and sleeve gastrectomy (SG).[65] On the other hand, in experiments using whole-body FXR knockout mice, vertical SG did not result in weight loss or a reduction in obesity control,[66] suggesting that RYGB and SG involve altered gut microbiota and BA signaling. It is also interesting to note that porphyran administration increased gut microbiota in a similar way to RYGB in the present study. Further studies are required to identify the specific species of gut microbiota altered by porphyran administration and to determine whether fecal transplantation of gut microbiota from the porphyran group into the HFD group improves this phenotype.

Porphyran administration changed BA composition

CDCA, a potent agonist for FXR, was decreased by porphyran treatment, along with secondary BAs. However, 3-dehydro-CDCA,[67] an intermediate in CDCA metabolism by the gut microbiota, was dramatically increased following porphyran administration. CDCA is synthesized in the liver and secreted into the intestine, where it undergoes dehydroxylation by the gut microbiota, and is eventually metabolized into the secondary BA LCA.[68] In the feces of mice fed porphyran derived from discolored nori, 3-dehydro-CDCA levels were elevated. This suggests either an increase in gut microbiota that facilitate the conversion of CDCA to 3-dehydro-CDCA or a decrease in those that convert 3-dehydro-CDCA to LCA. The specific gut microbiota responsible for these processes have yet to be identified.

In contrast, there was no increase in TβMCA, an FXR antagonist. In this study, downstream genes of FXR signaling in the intestine, such as *Fgf15* and *Ibabp*, were found to be reduced, indicating suppression of FXR signaling due to the reduced presence of FXR agonists. Since secondary BAs have been implicated in the development of HCC,[56] it is likely that the reduction in secondary BAs also contributed to the prevention of HCC development observed in this study. In the design of this study, animals were dissected in a fasted state to standardize metabolic conditions between groups. Therefore, BA secretion into the ileum was limited, and BA composition analysis was performed in feces. However, since FXR is located in the ileum, direct measurement of BA agonists and antagonists at this site would provide a more accurate insight. This will be the focus of future studies.

Porphyran administration changed intestinal FXR signal and ceramide synthesis

Consistent with previous studies, the expression of genes involved in ceramide synthesis, such as *Sptlc* and *Smpd*, decreased with the suppression of intestinal FXR signaling.[32] In fact, circulating ceramides in the blood were consistently reduced by porphyran treatment. The expression of genes involved in ceramide synthesis, such as *Sptlc* and *Smpd*, is regulated by FXR,[36] and it is thought that the suppression of intestinal

FXR reduced ceramide synthesis in the intestine, resulting in a decrease in the concentration of ceramide in the blood.

However, since blood ceramide levels are also influenced by ceramide synthesis in the liver, the porphyran-induced decrease in blood ceramide observed in this study should also be considered to indicate the inhibition of ceramide synthesis in the liver. In a previous study, intestinal FXR-deficient mice had an approximately 2-fold decrease in blood ceramide, and the effect of intestinal FXR deficiency on blood ceramide is expected to be high.[32] Ceramides are known to reduce lipid synthesis in the liver and have been shown to be effective in preventing conditions such as MASLD, MASH, and HCC. In the present study, porphyran administration also reduced hepatic lipid accumulation and prevented MetS, MASLD, MASH, and HCC. Conversely, it has been demonstrated that ceramide administration exacerbates obesity and insulin resistance[31] and fatty liver.[32] Moreover, a reduction in ceramide levels has been shown to exert disease-preventive effects.[69]

Previous studies have indicated that plant-derived compounds inhibit MASH by suppressing intestinal FXR signaling. For example, astragaloside, which contains polysaccharides similar to porphyran, and caffeic acid phenethyl ester, commonly found in many plants, are thought to suppress intestinal FXR by inhibiting the enzyme bile salt hydrolase, which causes alterations in the gut microbiota and promotes BA dehydration.[70] Additionally, caffeic acid phenethyl ester has been proposed as a potential inhibitor of intestinal bacterial growth.[71] Conversely, compounds such as betulinic acid and caffeic acid phenethyl ester, derived from the bark of *Betula vulgaris*, have demonstrated the capacity to exert FXR antagonist effects independently. Research into the potential of naturally occurring substances to modulate intestinal FXR activity, whether directly or indirectly, is ongoing. These substances have been shown to suppress intestinal FXR and inhibit fatty acid synthesis in the liver by reducing ceramide synthesis, thereby improving MASH.

Limitations of the study

The findings of this study indicate that porphyran treatment induces a notable reduction in body weight, suggesting that the decrease in adipose tissue may have contributed to improved glycemic control and reduced ceramide synthesis. However, in the MASH and HCC models, the porphyran group exhibited suppression of intestinal FXR signaling and decreased expression of ceramide synthesis-related genes, even in the absence of weight loss. These findings suggest that the effects of porphyran may be at least partially direct. This study is significant because it showed that functional substances derived from foods prevent MetS, MASLD, MASH, and HCC via the gut microbiota-BA-ceramide pathway and helped clarify the black box between the gut microbiota and disease.

Further research is needed to establish the proposed intestinal FXR-ceramide pathway as a major mechanism. It remains possible that the decrease in ceramide synthesis in the liver is a contributing factor. It is also possible that gut microbiota metabolites other than BAs may be involved in the preventive effect of porphyran in this study, and further studies are needed. In addition to porphyran administration, the administration of ceramide may help to clarify the extent to which ceramide synthesis reduction contributes to the disease-preventive effect of porphyran and to deepen our knowledge of whether changes in the intestinal microbiota caused by porphyran administration also contribute to its preventive effect.

Of note, our study primarily addressed preventive rather than therapeutic applications. Further research should investigate the potential therapeutic application of porphyran in disease models, such as obesity, to evaluate its efficacy in treatment. Furthermore, generalization of results beyond gender is limited as only male mice were used in this experiment.

Utilization of discolored nori and global environmental sustainability

The porphyran used in this study was extracted from discarded discolored nori, which is discarded due to loss of color. Previous studies have indicated that porphyrans in normal nori and those in discarded discolored nori differ in molecular weight and anti-inflammatory properties.[13] It is reported that 16.7 tons of discolored nori were disposed of in one of Japan's 47 prefectures in 6 months.[72,73] In recent years, scientific research on the re-use of waste reutilization has advanced significantly, particularly regarding seaweed waste, which has been extensively studied for applications in biosorbents, biofuels, and fertilizers (Figures S11 and S12; Table S3). In the meantime, studies on health-promoting and disease-preventive effects have been lacking (Figures S11 and S12; Table S3). In contrast, this study presents the possibility of meeting global environmental sustainability and addressing unmet medical needs.

RESOURCE AVAILABILITY

Lead contact

Requests for further information and resources should be directed to and will be fulfilled by the lead contact, Yoko Yokoyama (wmitsulab@gmail.com).

Materials availability

This study did not generate new unique reagents.

Data and code availability

- The transcriptome data have been deposited at gene expression omnibus database (GEO, https://www.ncbi.nlm.nih.gov/gds): GSE 166440 and are publicly available as of the date of publication.
- The microbiome analysis data have been deposited at the DNA DataBank of Japan (DDBJ) Sequence Read Archive (https://www.ddbj.nig.ac.jp): DRA014266 and are publicly available as of the date of publication.
- This paper does not report original code.
- Any additional information required to reanalyze the data reported in this paper is available from the lead contact upon request.

ACKNOWLEDGMENTS

We thank the scientists from the J.A. lab for comments and discussions. The authors also acknowledge the support of Health Science Lab Laboratories at Shonan Keiiku Hospital, the Fourth Laboratory of the Department of Pathology and the Collaborative Research Resources at Keio University School of Medicine for assistance with technical support.

This study was supported by JSPS KAKENHI grant number JP16H05292 (M.W.), JSPS KAKENHI grant numbers JP19K11751 and JP22K11709 (Y.Y.), JSPS KAKENHI grant number 22H03541 (S.F.), Japan Agency for Medical Research and Development (AMED) under grant number JP22fk0210073 (M.W.), Japan Agency for Medical Research and Development (AMED) under

grant number JP25fk0210129 (M.W.), Japan Agency for Medical Research and Development (AMED) under grant number JP22gm1010009 (S.F.), JST ERATO under grant number JPMJER1902 (S.F.), Food Science Institute Foundation (S.F.), École Polytechnique Fédérale de Lausanne (EPFL) (J.A.), GRL grant of the National Research Foundation of Korea (NRF 2017K1A1A2013124) (J.A.), and Agriculture, Forestry and Fisheries Research Council (Ministry of Agriculture, Forestry and Fisheries of Japan) (K.I. and M.W.). Longevity Initiative of the Program for the Advancement of Research in Core Projects at the Keio University Global Research Institute (KGRI) (K.T. and M.W.). Academic Development Funds research funding, Keio University (M.W.). Academic Exchange Grants, Keio University (M.W.).

AUTHOR CONTRIBUTIONS

Conceptualization, A.S., K.I., K.T., and M.W.; investigation, Y.Y., Y.T., J.-D.M., T. Taworntawat, N.K., U.N., T. Tanigaki, A.N., T.M., H.T., A.M., A.P., N.S., S.T., S.F., A.H., M.A., J.A., and M.W.; visualization, Y.Y., J.-D.M., T. Taworntawat, and U.N.; supervision, J.A. and M.W.; writing – original draft, Y.Y., Y.T., J.-D.M., J.A., and M.W.; writing – review and editing, T. Taworntawat, N.K., U.N., T. Tanigaki, A.N., T.M., H.T., A.M., A.P., A.S., N.S., S.T., S.F., A.H., K.I., M.A., and K.T.

DECLARATION OF INTERESTS

The authors declare no competing interests.

STAR★METHODS

Detailed methods are provided in the online version of this paper and include the following:

- KEY RESOURCES TABLE
- EXPERIMENTAL MODEL AND STUDY PARTICIPANT DETAILS
  - Mice
- METHOD DETAILS
  - Diet-induced obesity mouse model
  - MASH mouse model
  - HCC mouse model
  - Extraction and quality control of porphyran
  - Liver lipid extractions
  - Assay for plasma and liver metabolic parameters
  - Histopathology on obesity model mice liver tissues
  - Oral glucose tolerance test (OGTT)
  - Intraperitoneal insulin tolerance test (IPITT)
  - RNA extraction and quantitative RT-PCR
  - Transcriptome analysis
  - 16S rRNA gene sequencing
  - Cholesterol composition
  - FFA composition
  - Ceramide analysis
  - Plasma ALT and AST
  - Histopathology on MASH model mouse liver tissues
  - Bile acid analysis
  - Literature review of studies on seaweed waste
- QUANTIFICATION AND STATISTICAL ANALYSIS

SUPPLEMENTAL INFORMATION

Supplemental information can be found online at https://doi.org/10.1016/j.isci.2025.112603.

Received: November 18, 2024
Revised: March 10, 2025
Accepted: May 2, 2025
Published: May 7, 2025

REFERENCES

1. Riazi, K., Azhari, H., Charette, J.H., Underwood, F.E., King, J.A., Afshar, E. E., Swain, M.G., Congly, S.E., Kaplan, G.G., and Shaheen, A.A. (2022). The prevalence and incidence of NAFLD worldwide: a systematic review and meta-analysis. Lancet Gastroenterol. Hepatol. *7*, 851–861. https://doi.org/10.1016/S2468-1253(22)00165-0.
2. Younossi, Z.M., Otgonsuren, M., Henry, L., Venkatesan, C., Mishra, A., Erario, M., and Hunt, S. (2015). Association of nonalcoholic fatty liver disease (NAFLD) with hepatocellular carcinoma (HCC) in the United States from 2004 to 2009. Hepatology *62*, 1723–1730. https://doi.org/10.1002/hep.28123.
3. Harrison, S.A., Allen, A.M., Dubourg, J., Noureddin, M., and Alkhouri, N. (2023). Challenges and opportunities in NASH drug development. Nat. Med. *29*, 562–573. https://doi.org/10.1038/s41591-023-02242-6.
4. Francque, S., Krag, A., Shawcross, D.L., and Zelber-Sagi, S. (2024). A turning point in hepatology? EASL reflects on the first approved drug for MASH. J. Hepatol. *81*, 192–194. https://doi.org/10.1016/j.jhep.2024.04.036.
5. OECD (2017). Obesity update. https://www.oecd.org/els/health-systems/Obesity-Update-2017.pdf.
6. United Nations Population Division (2017). World Population Prospects: The 2017 Revision (United Nations). https://esa.un.org/unpd/wpp.
7. Estes, C., Anstee, Q.M., Arias-Loste, M.T., Bantel, H., Bellentani, S., Caballeria, J., Colombo, M., Craxi, A., Crespo, J., Day, C.P., et al. (2018). Modeling NAFLD disease burden in China, France, Germany, Italy, Japan, Spain, United Kingdom, and United States for the period 2016-2030. J. Hepatol. *69*, 896–904. https://doi.org/10.1016/j.jhep.2018.05.036.
8. GBD 2017 Diet Collaborators (2019). Health effects of dietary risks in 195 countries, 1990-2017: a systematic analysis for the Global Burden of Disease Study 2017. Lancet *393*, 1958–1972. https://doi.org/10.1016/S0140-6736(19)30041-8.
9. Mokdad, A.H., Marks, J.S., Stroup, D.F., and Gerberding, J.L. (2004). Actual causes of death in the United States, 2000. JAMA *291*, 1238–1245. https://doi.org/10.1001/jama.291.10.1238.
10. Sasaki, S.; for Working Group 1 of the Healthy Diet Research Committee of International Life Sciences Institute Japan (2020). What is the scientific definition of the Japanese diet from the viewpoint of nutrition and health? Nutr. Rev. *78*, 18–26. https://doi.org/10.1093/nutrit/nuaa099.
11. Brown, E.S., Allsopp, P.J., Magee, P.J., Gill, C.I.R., Nitecki, S., Strain, C. R., and McSorley, E.M. (2014). Seaweed and human health. Nutr. Rev. *72*, 205–216. https://doi.org/10.1111/nure.12091.
12. Ishihara, K., Seko, T., Oyamada, C., Kunitake, H., and Muraoka, T. (2021). Synergistic effect of dietary glycerol galactoside and porphyran from nori on cecal immunoglobulin A levels in mice. Food Sci. Technol. Res. *27*, 95–101. https://doi.org/10.3136/fstr.27.95.
13. Isaka, S., Cho, K., Nakazono, S., Abu, R., Ueno, M., Kim, D., and Oda, T. (2015). Antioxidant and anti-inflammatory activities of porphyran isolated from discolored nori (Porphyra yezoensis). Int. J. Biol. Macromol. *74*, 68–75. https://doi.org/10.1016/j.ijbiomac.2014.11.043.
14. Nishiguchi, T., Cho, K., Isaka, S., Ueno, M., Jin, J.O., Yamaguchi, K., Kim, D., and Oda, T. (2016). Protective effect of porphyran isolated from discolored nori (Porphyra yezoensis) on lipopolysaccharide-induced endotoxin shock in mice. Int. J. Biol. Macromol. *93*, 1273–1278. https://doi.org/10.1016/j.ijbiomac.2016.09.091.
15. Ahmad, T.R., and Haeusler, R.A. (2019). Bile acids in glucose metabolism and insulin signalling - mechanisms and research needs. Nat. Rev. Endocrinol. *15*, 701–712. https://doi.org/10.1038/s41574-019-0266-7.
16. Watanabe, M., Houten, S.M., Wang, L., Moschetta, A., Mangelsdorf, D.J., Heyman, R.A., Moore, D.D., and Auwerx, J. (2004). Bile acids lower triglyceride levels via a pathway involving FXR, SHP, and SREBP-1c. J. Clin. Investig. *113*, 1408–1418. https://doi.org/10.1172/JCI21025.

17. Watanabe, M., Houten, S.M., Mataki, C., Christoffolete, M.A., Kim, B.W., Sato, H., Messaddeq, N., Harney, J.W., Ezaki, O., Kodama, T., et al. (2006). Bile acids induce energy expenditure by promoting intracellular thyroid hormone activation. Nature *439*, 484–489. https://doi.org/10.1038/nature04330.

18. Houten, S.M., Watanabe, M., and Auwerx, J. (2006). Endocrine functions of bile acids. EMBO J. *25*, 1419–1425. https://doi.org/10.1038/sj.emboj.7601049.

19. Moore, D.D., Kato, S., Xie, W., Mangelsdorf, D.J., Schmidt, D.R., Xiao, R., and Kliewer, S.A. (2006). International Union of Pharmacology. LXII. The NR1H and NR1I receptors: constitutive androstane receptor, pregnene X receptor, farnesoid X receptor alpha, farnesoid X receptor beta, liver X receptor alpha, liver X receptor beta, and vitamin D receptor. Pharmacol. Rev. *58*, 742–759. https://doi.org/10.1124/pr.58.4.6.

20. Perino, A., Demagny, H., Velazquez-Villegas, L., and Schoonjans, K. (2021). Molecular Physiology of Bile Acid Signaling in Health, Disease, and Aging. Physiol. Rev. *101*, 683–731. https://doi.org/10.1152/physrev.00049.2019.

21. Perino, A., and Schoonjans, K. (2022). Metabolic Messengers: bile acids. Nat. Metab. *4*, 416–423. https://doi.org/10.1038/s42255-022-00559-z.

22. Handelsman, Y. (2011). Role of bile acid sequestrants in the treatment of type 2 diabetes. Diabetes Care *34*, S244–S250. https://doi.org/10.2337/dc11-s237.

23. Watanabe, M., Morimoto, K., Houten, S.M., Kaneko-Iwasaki, N., Sugizaki, T., Horai, Y., Mataki, C., Sato, H., Murahashi, K., Arita, E., et al. (2012). Bile acid binding resin improves metabolic control through the induction of energy expenditure. PLoS One *7*, e38286. https://doi.org/10.1371/journal.pone.0038286.

24. Watanabe, M., Horai, Y., Houten, S.M., Morimoto, K., Sugizaki, T., Arita, E., Mataki, C., Sato, H., Tanigawara, Y., Schoonjans, K., et al. (2011). Lowering bile acid pool size with a synthetic farnesoid X receptor (FXR) agonist induces obesity and diabetes through reduced energy expenditure. J. Biol. Chem. *286*, 26913–26920. https://doi.org/10.1074/jbc.M111.248203.

25. Miyata, M., Hata, T., Yamakawa, H., Kagawa, T., Yoshinari, K., and Yamazoe, Y. (2012). Involvement of multiple elements in FXR-mediated transcriptional activation of FGF19. J. Steroid Biochem. Mol. Biol. *132*, 41–47. https://doi.org/10.1016/j.jsbmb.2012.04.008.

26. Morimoto, K., Watanabe, M., Sugizaki, T., Irie, J.i., and Itoh, H. (2016). Intestinal Bile Acid Composition Modulates Prohormone Convertase 1/3 (PC1/3) Expression and Consequent GLP-1 Production in Male Mice. Endocrinology *157*, 1071–1081. https://doi.org/10.1210/en.2015-1551.

27. Fang, S., Suh, J.M., Reilly, S.M., Yu, E., Osborn, O., Lackey, D., Yoshihara, E., Perino, A., Jacinto, S., Lukasheva, Y., et al. (2015). Intestinal FXR agonism promotes adipose tissue browning and reduces obesity and insulin resistance. Nat. Med. *21*, 159–165. https://doi.org/10.1038/nm.3760.

28. Kawamata, Y., Fujii, R., Hosoya, M., Harada, M., Yoshida, H., Miwa, M., Fukusumi, S., Habata, Y., Itoh, T., Shintani, Y., et al. (2003). A G protein-coupled receptor responsive to bile acids. J. Biol. Chem. *278*, 9435–9440. https://doi.org/10.1074/jbc.M209706200.

29. Thomas, C., Gioiello, A., Noriega, L., Strehle, A., Oury, J., Rizzo, G., Macchiarulo, A., Yamamoto, H., Mataki, C., Pruzanski, M., et al. (2009). TGR5-mediated bile acid sensing controls glucose homeostasis. Cell Metab. *10*, 167–177. https://doi.org/10.1016/j.cmet.2009.08.001.

30. Pathak, P., Xie, C., Nichols, R.G., Ferrell, J.M., Boehme, S., Krausz, K.W., Patterson, A.D., Gonzalez, F.J., and Chiang, J.Y.L. (2018). Intestine farnesoid X receptor agonist and the gut microbiota activate G-protein bile acid receptor-1 signaling to improve metabolism. Hepatology *68*, 1574–1588. https://doi.org/10.1002/hep.29857.

31. Jiang, C., Xie, C., Lv, Y., Li, J., Krausz, K.W., Shi, J., Brocker, C.N., Desai, D., Amin, S.G., Bisson, W.H., et al. (2015). Intestine-selective farnesoid X receptor inhibition improves obesity-related metabolic dysfunction. Nat. Commun. *6*, 10166. https://doi.org/10.1038/ncomms10166.

32. Jiang, C., Xie, C., Li, F., Zhang, L., Nichols, R.G., Krausz, K.W., Cai, J., Qi, Y., Fang, Z.Z., Takahashi, S., et al. (2015). Intestinal farnesoid X receptor signaling promotes nonalcoholic fatty liver disease. J. Clin. Investig. *125*, 386–402. https://doi.org/10.1172/JCI76738.

33. Xia, J.Y., Holland, W.L., Kusminski, C.M., Sun, K., Sharma, A.X., Pearson, M.J., Sifuentes, A.J., McDonald, J.G., Gordillo, R., and Scherer, P.E. (2015). Targeted Induction of Ceramide Degradation Leads to Improved Systemic Metabolism and Reduced Hepatic Steatosis. Cell Metab. *22*, 266–278. https://doi.org/10.1016/j.cmet.2015.06.007.

34. Raichur, S., Wang, S.T., Chan, P.W., Li, Y., Ching, J., Chaurasia, B., Dogra, S., Öhman, M.K., Takeda, K., Sugii, S., et al. (2014). CerS2 haploinsufficiency inhibits beta-oxidation and confers susceptibility to diet-induced steatohepatitis and insulin resistance. Cell Metab. *20*, 687–695. https://doi.org/10.1016/j.cmet.2014.09.015.

35. Jiang, J., Ma, Y., Liu, Y., Lu, D., Gao, X., Krausz, K.W., Desai, D., Amin, S.G., Patterson, A.D., Gonzalez, F.J., and Xie, C. (2022). Glycine-beta-muricholic acid antagonizes the intestinal farnesoid X receptor-ceramide axis and ameliorates NASH in mice. Hepatol. Commun. *6*, 3363–3378. https://doi.org/10.1002/hep4.2099.

36. Gonzalez, F.J., Jiang, C., and Patterson, A.D. (2016). An Intestinal Microbiota-Farnesoid X Receptor Axis Modulates Metabolic Disease. Gastroenterology *151*, 845–859. https://doi.org/10.1053/j.gastro.2016.08.057.

37. National Library of Medicine (2024). PubChem Identifier, CID 163304497. https://pubchem.ncbi.nlm.nih.gov/compound/Porphyran.

38. Chun, K.H. (2021). Mouse model of the adipose organ: the heterogeneous anatomical characteristics. Arch Pharm. Res. (Seoul) *44*, 857–875. https://doi.org/10.1007/s12272-021-01350-6.

39. Shepherd, E.S., DeLoache, W.C., Pruss, K.M., Whitaker, W.R., and Sonnenburg, J.L. (2018). An exclusive metabolic niche enables strain engraftment in the gut microbiota. Nature *557*, 434–438. https://doi.org/10.1038/s41586-018-0092-4.

40. Haus, J.M., Kashyap, S.R., Kasumov, T., Zhang, R., Kelly, K.R., Defronzo, R.A., and Kirwan, J.P. (2009). Plasma ceramides are elevated in obese subjects with type 2 diabetes and correlate with the severity of insulin resistance. Diabetes *58*, 337–343. https://doi.org/10.2337/db08-1228.

41. Wigger, L., Cruciani-Guglielmacci, C., Nicolas, A., Denom, J., Fernandez, N., Fumeron, F., Marques-Vidal, P., Ktorza, A., Kramer, W., Schulte, A., et al. (2017). Plasma Dihydroceramides Are Diabetes Susceptibility Biomarker Candidates in Mice and Humans. Cell Rep. *18*, 2269–2279. https://doi.org/10.1016/j.celrep.2017.02.019.

42. Kurz, J., Parnham, M.J., Geisslinger, G., and Schiffmann, S. (2019). Ceramides as Novel Disease Biomarkers. Trends Mol. Med. *25*, 20–32. https://doi.org/10.1016/j.molmed.2018.10.009.

43. Paul, B., Lewinska, M., and Andersen, J.B. (2022). Lipid alterations in chronic liver disease and liver cancer. JHEP Rep. *4*, 100479. https://doi.org/10.1016/j.jhepr.2022.100479.

44. Laurila, P.P., Luan, P., Wohlwend, M., Zanou, N., Crisol, B., Imamura de Lima, T., Goeminne, L.J.E., Gallart-Ayala, H., Shong, M., Ivanisevic, J., et al. (2022). Inhibition of sphingolipid *de novo* synthesis counteracts muscular dystrophy. Sci. Adv. *8*, eabh4423. https://doi.org/10.1126/sciadv.abh4423.

45. Summers, S.A. (2018). Could Ceramides Become the New Cholesterol? Cell Metab. *27*, 276–280. https://doi.org/10.1016/j.cmet.2017.12.003.

46. Sun, L., Cai, J., and Gonzalez, F.J. (2021). The role of farnesoid X receptor in metabolic diseases, and gastrointestinal and liver cancer. Nat. Rev. Gastroenterol. Hepatol. *18*, 335–347. https://doi.org/10.1038/s41575-020-00404-2.

47. Janowski, B.A., Willy, P.J., Devi, T.R., Falck, J.R., and Mangelsdorf, D.J. (1996). An oxysterol signalling pathway mediated by the nuclear receptor LXR alpha. Nature *383*, 728–731. https://doi.org/10.1038/383728a0.

48. Janowski, B.A., Grogan, M.J., Jones, S.A., Wisely, G.B., Kliewer, S.A., Corey, E.J., and Mangelsdorf, D.J. (1999). Structural requirements of

ligands for the oxysterol liver X receptors LXRalpha and LXRbeta. Proc. Natl. Acad. Sci. USA *96*, 266–271. https://doi.org/10.1073/pnas.96.1.266.

49. Lehmann, J.M., Kliewer, S.A., Moore, L.B., Smith-Oliver, T.A., Oliver, B.B., Su, J.L., Sundseth, S.S., Winegar, D.A., Blanchard, D.E., Spencer, T.A., and Willson, T.M. (1997). Activation of the nuclear receptor LXR by oxysterols defines a new hormone response pathway. J. Biol. Chem. *272*, 3137–3140. https://doi.org/10.1074/jbc.272.6.3137.

50. Sugizaki, T., Watanabe, M., Horai, Y., Kaneko-Iwasaki, N., Arita, E., Miyazaki, T., Morimoto, K., Honda, A., Irie, J., and Itoh, H. (2014). The Niemann-Pick C1 like 1 (NPC1L1) inhibitor ezetimibe improves metabolic disease via decreased liver X receptor (LXR) activity in liver of obese male mice. Endocrinology *155*, 2810–2819. https://doi.org/10.1210/en.2013-2143.

51. Hannun, Y.A., and Obeid, L.M. (2002). The Ceramide-centric universe of lipid-mediated cell regulation: stress encounters of the lipid kind. J. Biol. Chem. *277*, 25847–25850. https://doi.org/10.1074/jbc.R200008200.

52. Linn, S.C., Kim, H.S., Keane, E.M., Andras, L.M., Wang, E., and Merrill, A. H., Jr. (2001). Regulation of *de novo* sphingolipid biosynthesis and the toxic consequences of its disruption. Biochem. Soc. Trans. *29*, 831–835. https://doi.org/10.1042/0300-5127:0290831.

53. Simon, J., Ouro, A., Ala-Ibanibo, L., Presa, N., Delgado, T.C., and Martínez-Chantar, M.L. (2019). Sphingolipids in Non-Alcoholic Fatty Liver Disease and Hepatocellular Carcinoma: Ceramide Turnover. Int. J. Mol. Sci. *21*, 40. https://doi.org/10.3390/ijms21010040.

54. Ni, Y., Nagashimada, M., Zhuge, F., Zhan, L., Nagata, N., Tsutsui, A., Nakanuma, Y., Kaneko, S., and Ota, T. (2015). Astaxanthin prevents and reverses diet-induced insulin resistance and steatohepatitis in mice: A comparison with vitamin E. Sci. Rep. *5*, 17192. https://doi.org/10.1038/srep17192.

55. Zou, A., Magee, N., Deng, F., Lehn, S., Zhong, C., and Zhang, Y. (2018). Hepatocyte nuclear receptor SHP suppresses inflammation and fibrosis in a mouse model of nonalcoholic steatohepatitis. J. Biol. Chem. *293*, 8656–8671. https://doi.org/10.1074/jbc.RA117.001653.

56. Yoshimoto, S., Loo, T.M., Atarashi, K., Kanda, H., Sato, S., Oyadomari, S., Iwakura, Y., Oshima, K., Morita, H., Hattori, M., et al. (2013). Obesity-induced gut microbial metabolite promotes liver cancer through senescence secretome. Nature *499*, 97–101. https://doi.org/10.1038/nature12347.

57. Turpin, S.M., Nicholls, H.T., Willmes, D.M., Mourier, A., Brodesser, S., Wunderlich, C.M., Mauer, J., Xu, E., Hammerschmidt, P., Brönneke, H. S., et al. (2014). Obesity-induced CerS6-dependent C16:0 ceramide production promotes weight gain and glucose intolerance. Cell Metab. *20*, 678–686. https://doi.org/10.1016/j.cmet.2014.08.002.

58. de Vos, W.M., Tilg, H., Van Hul, M., and Cani, P.D. (2022). Gut microbiome and health: mechanistic insights. Gut *71*, 1020–1032. https://doi.org/10.1136/gutjnl-2021-326789.

59. Shen, F., Zheng, R.D., Sun, X.Q., Ding, W.J., Wang, X.Y., and Fan, J.G. (2017). Gut microbiota dysbiosis in patients with non-alcoholic fatty liver disease. Hepatobiliary Pancreat. Dis. Int. *16*, 375–381. https://doi.org/10.1016/S1499-3872(17)60019-5.

60. Boursier, J., Mueller, O., Barret, M., Machado, M., Fizanne, L., Araujo-Perez, F., Guy, C.D., Seed, P.C., Rawls, J.F., David, L.A., et al. (2016). The severity of nonalcoholic fatty liver disease is associated with gut dysbiosis and shift in the metabolic function of the gut microbiota. Hepatology *63*, 764–775. https://doi.org/10.1002/hep.28356.

61. Yu, J., Chen, X., Yang, X., and Zhang, B. (2024). Understanding gut dysbiosis for hepatocellular carcinoma diagnosis and treatment. Trends Endocrinol. Metab. *35*, 1006–1020. https://doi.org/10.1016/j.tem.2024.06.003.

62. Tintelnot, J., Xu, Y., Lesker, T.R., Schönlein, M., Konczalla, L., Giannou, A. D., Pelczar, P., Kylies, D., Puelles, V.G., Bielecka, A.A., et al. (2023). Microbiota-derived 3-IAA influences chemotherapy efficacy in pancreatic cancer. Nature *615*, 168–174. https://doi.org/10.1038/s41586-023-05728-y.

63. Johnson, E.L., Heaver, S.L., Waters, J.L., Kim, B.I., Bretin, A., Goodman, A.L., Gewirtz, A.T., Worgall, T.S., and Ley, R.E. (2020). Sphingolipids produced by gut bacteria enter host metabolic pathways impacting ceramide levels. Nat. Commun. *11*, 2471. https://doi.org/10.1038/s41467-020-16274-w.

64. Wang, C., Zhang, H., Liu, H., Zhang, H., Bao, Y., Di, J., and Hu, C. (2020). The genus Sutterella is a potential contributor to glucose metabolism improvement after Roux-en-Y gastric bypass surgery in T2D. Diabetes Res. Clin. Pract. *162*, 108116. https://doi.org/10.1016/j.diabres.2020.108116.

65. Poss, A.M., Krick, B., Maschek, J.A., Haaland, B., Cox, J.E., Karra, P., Ibele, A.R., Hunt, S.C., Adams, T.D., Holland, W.L., et al. (2022). Following Roux-en-Y gastric bypass surgery, serum ceramides demarcate patients that will fail to achieve normoglycemia and diabetes remission. Med *3*, 452–467.e4. https://doi.org/10.1016/j.medj.2022.05.011.

66. Ryan, K.K., Tremaroli, V., Clemmensen, C., Kovatcheva-Datchary, P., Myronovych, A., Karns, R., Wilson-Pérez, H.E., Sandoval, D.A., Kohli, R., Bäckhed, F., and Seeley, R.J. (2014). FXR is a molecular target for the effects of vertical sleeve gastrectomy. Nature *509*, 183–188. https://doi.org/10.1038/nature13135.

67. Kang, D.J., Ridlon, J.M., Moore, D.R., 2nd, Barnes, S., and Hylemon, P.B. (2008). Clostridium scindens baiCD and baiH genes encode stereospecific 7alpha/7beta-hydroxy-3-oxo-delta4-cholenoic acid oxidoreductases. Biochim. Biophys. Acta *1781*, 16–25. https://doi.org/10.1016/j.bbalip.2007.10.008.

68. Heinken, A., Ravcheev, D.A., Baldini, F., Heirendt, L., Fleming, R.M.T., and Thiele, I. (2019). Systematic assessment of secondary bile acid metabolism in gut microbes reveals distinct metabolic capabilities in inflammatory bowel disease. Microbiome *7*, 75. https://doi.org/10.1186/s40168-019-0689-3.

69. Chaurasia, B., Tippetts, T.S., Mayoral Monibas, R., Liu, J., Li, Y., Wang, L., Wilkerson, J.L., Sweeney, C.R., Pereira, R.F., Sumida, D.H., et al. (2019). Targeting a ceramide double bond improves insulin resistance and hepatic steatosis. Science *365*, 386–392. https://doi.org/10.1126/science.aav3722.

70. Adhikari, A.A., Seegar, T.C.M., Ficarro, S.B., McCurry, M.D., Ramachandran, D., Yao, L., Chaudhari, S.N., Ndousse-Fetter, S., Banks, A.S., Marto, J.A., et al. (2020). Development of a covalent inhibitor of gut bacterial bile salt hydrolases. Nat. Chem. Biol. *16*, 318–326. https://doi.org/10.1038/s41589-020-0467-3.

71. Zhong, X.C., Liu, Y.M., Gao, X.X., Krausz, K.W., Niu, B., Gonzalez, F.J., and Xie, C. (2023). Caffeic acid phenethyl ester suppresses intestinal FXR signaling and ameliorates nonalcoholic fatty liver disease by inhibiting bacterial bile salt hydrolase activity. Acta Pharmacol. Sin. *44*, 145–156. https://doi.org/10.1038/s41401-022-00921-7.

72. Sasuga, K., Yamanashi, T., Nakayama, S., Ono, S., and Mikami, K. (2018). Discolored Red Seaweed Pyropia yezoensis with Low Commercial Value Is a Novel Resource for Production of Agar Polysaccharides. Mar. Biotechnol. *20*, 520–530. https://doi.org/10.1007/s10126-018-9823-7.

73. Sugano, A., Sawano, M., and Inoue, S. (2009). The New Extracting Method of Functional Material Porpyran from Discoloration Laver. Bulletin of the Society of Sea Water Science, Japan *63*, 377–380.

74. Trevaskis, J.L., Griffin, P.S., Wittmer, C., Neuschwander-Tetri, B.A., Brunt, E.M., Dolman, C.S., Erickson, M.R., Napora, J., Parkes, D.G., and Roth, J. D. (2012). Glucagon-like peptide-1 receptor agonism improves metabolic, biochemical, and histopathological indices of nonalcoholic steatohepatitis in mice. Am. J. Physiol. Gastrointest. Liver Physiol. *302*, G762–G772. https://doi.org/10.1152/ajpgi.00476.2011.

75. Clapper, J.R., Hendricks, M.D., Gu, G., Wittmer, C., Dolman, C.S., Herich, J., Athanacio, J., Villescaz, C., Ghosh, S.S., Heilig, J.S., et al. (2013). Diet-induced mouse model of fatty liver disease and nonalcoholic steatohepatitis reflecting clinical disease progression and methods of assessment. Am. J. Physiol. Gastrointest. Liver Physiol. *305*, G483–G495. https://doi.org/10.1152/ajpgi.00079.2013.

76. Muraoka, T., Ishihara, K., Oyamada, C., Kunitake, H., Hirayama, I., and Kimura, T. (2008). Fermentation properties of low-quality red alga Susabinori Porphyra yezoensis by intestinal bacteria. Biosci. Biotechnol. Biochem. *72*, 1731–1739. https://doi.org/10.1271/bbb.80029.

77. Ishihara, K., Oyamada, C., Sato, Y., Danno, H., Kimiya, T., Kaneniwa, M., Kunitake, H., and Muraoka, T. (2008). Relationships between quality parameters and content of glycerol galactoside and porphyra-334 in dried laver nori Porphyra yezoensis. Fish. Sci. *74*, 167–173. https://doi.org/10.1111/j.1444-2906.2007.01506.x.

78. Folch, J., Lees, M., and Sloane Stanley, G.H. (1957). A simple method for the isolation and purification of total lipides from animal tissues. J. Biol. Chem. *226*, 497–509.

79. Andrikopoulos, S., Blair, A.R., Deluca, N., Fam, B.C., and Proietto, J. (2008). Evaluating the glucose tolerance test in mice. Am. J. Physiol. Endocrinol. Metab. *295*, E1323–E1332. https://doi.org/10.1152/ajpendo.90617.2008.

80. Cozar-Castellano, I., and Perdomo, G. (2020). Assessment of Insulin Tolerance In Vivo in Mice. Methods Mol. Biol. *2128*, 217–224. https://doi.org/10.1007/978-1-0716-0385-7_15.

81. Honda, A., Yamashita, K., Hara, T., Ikegami, T., Miyazaki, T., Shirai, M., Xu, G., Numazawa, M., and Matsuzaki, Y. (2009). Highly sensitive quantification of key regulatory oxysterols in biological samples by LC-ESI-MS/MS. J. Lipid Res. *50*, 350–357. https://doi.org/10.1194/jlr.D800040-JLR200.

82. Honda, A., Yamashita, K., Miyazaki, H., Shirai, M., Ikegami, T., Xu, G., Numazawa, M., Hara, T., and Matsuzaki, Y. (2008). Highly sensitive analysis of sterol profiles in human serum by LC-ESI-MS/MS. J. Lipid Res. *49*, 2063–2073. https://doi.org/10.1194/jlr.D800017-JLR200.

83. Tsugawa, H., Ikeda, K., Tanaka, W., Senoo, Y., Arita, M., and Arita, M. (2017). Comprehensive identification of sphingolipid species by in silico retention time and tandem mass spectral library. J. Cheminform. *9*, 19. https://doi.org/10.1186/s13321-017-0205-3.

84. Schneider, C.A., Rasband, W.S., and Eliceiri, K.W. (2012). NIH Image to ImageJ: 25 years of image analysis. Nat. Methods *9*, 671–675. https://doi.org/10.1038/nmeth.2089.

85. Honda, A., Miyazaki, T., Iwamoto, J., Hirayama, T., Morishita, Y., Monma, T., Ueda, H., Mizuno, S., Sugiyama, F., Takahashi, S., and Ikegami, T. (2020). Regulation of bile acid metabolism in mouse models with hydrophobic bile acid composition. J. Lipid Res. *61*, 54–69. https://doi.org/10.1194/jlr.RA119000395.

86. Murakami, M., Iwamoto, J., Honda, A., Tsuji, T., Tamamushi, M., Ueda, H., Monma, T., Konishi, N., Yara, S., Hirayama, T., et al. (2018). Detection of Gut Dysbiosis due to Reduced Clostridium Subcluster XIVa Using the Fecal or Serum Bile Acid Profile. Inflamm. Bowel Dis. *24*, 1035–1044. https://doi.org/10.1093/ibd/izy022.

STAR★METHODS

KEY RESOURCES TABLE

REAGENT or RESOURCE	SOURCE	IDENTIFIER
Chemicals, peptides, and recombinant proteins		
7,12-dimethylbenz(a)anthracene	Sigma-Aldrich	Cat.#D3254
Insulin	Eli Lilly and Company	Humulin R U-100
Critical commercial assays		
Determiner L	Kyowa Medex	13A2X00172061001
NEFA C-test Wako	Wako Pure Chemical	16100AMZ04060000
T-cho test Wako	Wako Pure Chemical	27A2X00235000012
Mouse/Rat Leptin ELISA kit	Morinaga Institute of Biological Science, Inc.	Cat.#M1305
Mouse insulin ELISA kit	Morinaga Institute of Biological Science, Inc.	Cat.#M1104
GLP-1 ELISA kit	Immuno-Biological Laboratories Co., Ltd.	Cat.# 27784
Rneasy Mini kit	Qiagen	Cat.# 74106
PrimeScript RT Master Mix	Takara Bio, Inc.	Cat.# RR036A
SYBR Premix Ex TaqII	Takara Bio, Inc.	Cat.# RR820D
QIAamp PowerFecal Pro DNA Kit	Qiagen	Cat.# 51804
Alanine Aminotransferase Activity Assay Kit	Bio Vision Inc.	Cat.#K752-100
Aspartate Aminotransferase Activity Colorimetric Assay Kit	Bio Vision Inc.	Cat.#K753-100
Deposited data		
Gene Expression Omnibus	This paper	GSE166440
DNA DataBank of Japan (DDBJ)	This paper	DRA014266
Experimental models: Organisms/strains		
Mouse C57BL/6J	Japan SLC, Inc.	C57BL/6JmsSlc
Oligonucleotides		
Primers, see Table S1	This paper	N/A
Software and algorithms		
ImageJ Software	U. S. National Institutes of Health	https://imagej.net/software/ImageJ/
GraphPad Prism 10	Graphpad Software	https://www.graphpad.com/
R Software	R Software	https://www.r-project.org

EXPERIMENTAL MODEL AND STUDY PARTICIPANT DETAILS

Mice

WT (C57BL/6J) mice were kept under conventional conditions of controlled temperature, humidity, and lighting (12-h light/dark cycle with lights on at 8:00) and given free access to food and water. For obesity and MASH model, five-week old male C57BL/6J mice were used. For HCC model, three to five days old male C57BL/6J mice were used. All animal experiments were approved by the Institutional Animal Care and Use Committee of Keio University School of Medicine (no.15046, 19024 and 20072).

METHOD DETAILS

Diet-induced obesity mouse model

Five-week-old male C57BL/6J mice purchased from Japan SLC, Inc. (Shizuoka, Japan). After one week of acclimation, mice were randomly divided into four groups according to body weight: chow diet (CD) (Research Diets, Inc., NJ, USA, D12450B), high-fat diet (HFD) (Research Diets, Inc., NJ, USA, D12492), HFD with porphyran (2% w/w) (HFD-P) and HFD with nori extract (2% w/w) (HFD-Ex) *ad libitum* for 13 weeks. The body weight, food intake was measured once per week. The mice were harvesting of blood for subsequent lipid measurements, and tissues (liver, mWAT, ileum, colon and BAT) for RNA isolation, lipid measurements, and histology.

MASH mouse model

Five-week-old male C57BL/6J mice were purchased from Japan SLC, Inc. (Shizuoka, Japan). After one week of acclimation, mice were randomly divided into three groups according to body weight: control diet (CD) (Research Diets, Inc., NJ, USA, D09100304); high fat and high cholesterol diet (HFHCD) (Research Diets, Inc., NJ, USA, D09100301) and HFHCD diet supplemented with 2% w/w porphyran (HFHCD-P).[74,75] After 18 weeks, animals were anesthetized with isoflurane, blood and tissue were collected, and frozen in liquid nitrogen.

HCC mouse model

Three to five day old male C57BL/6J mice were treated topically with 50 μL of 0.5% tumorigenic 7,12-dimethylbenz(a)anthracene (DMBA, Sigma-Aldrich, MO, USA).[56] At 6 weeks of age, mice were randomly placed on control (CD + DMBA) (Research Diets, Inc., NJ, USA, D12450B), high-fat diet (HFD+DMBA) (Research Diets, Inc., NJ, USA, D12492) and HFD with porphyran (2% w/w) (HFD+DMBA-P) diets for 31 weeks.[56] After 31 weeks, animals were anesthetized with isoflurane, and blood and tissue were collected and frozen in liquid nitrogen.

Extraction and quality control of porphyran

Porphyran was extracted from discolored *Porphyra yezoensis* (currently *Neopyropia yezoensis*) as previously reported.[12] Glycerol galactoside (GG) was extracted from discolored nori by a previously described method.[76] HPLC confirmed GG purity and was over 95%.[77] Porphyran was extracted from the residue from which GG was extracted. Specifically, the GG extraction residue (about 300 g) was added to 0.5 L of water and autoclaved at 120°C for 30 min. Then, up to 5 L of water was added to the resulting solution and mixed at 5°C overnight. The extract was collected with a centrifugal dehydrator (H-122, Kokusan Co., Saitama, Japan) and concentrated to approximately 1 L with a rotary evaporator. Porphyran was precipitated from the concentrated extract by sequentially adding 1/10 volume of 3M sodium acetate and 3 volumes of ethanol; after centrifugation at 10000 X g for 15 min, the supernatant was discarded and the precipitate was dried under vacuum and ground to a white powder using a grinding mill 800DG (Iwatani Sangyo, Tokyo, Japan). Porphyran content of the discolored nori was 51.5% at dry basis (w/w) in average.

To examine the purity of the porphyran, the powder was hydrolyzed with 4M trifluoroacetic acid and then analyzed for sugar composition using ABEE Labeling Kit Plus S (J-Oil Mills, Tokyo, Japan). As a result, only galactose after acid degradation of sugars contained in porphyran was detected, and no acid degradation products of other sugars contained in discolored nori were detected. The main components of the discolored nori extract are porphyran and GG as sugar components. The discolored nori extract was ultrafiltrated (MWCO = 3000), and the sugar content was determined by the phenol sulfate method (standard was galactose). Porphyran content of the nori extract (porphyran content = sugar content of the extract - sugar content of the filtrate) greater than 60% was used as the discolored nori extract. Porphyran content of the nori extract powder was 67.7% at dry basis (w/w).

Liver lipid extractions

After experiments, liver was taken from mice and a section of liver (always from the same lobe) was used for lipid extraction. Lipid extracts were prepared by the classical Folch method.[78] Extracts were dried and resuspended in isopropanol.

Assay for plasma and liver metabolic parameters

Plasma and liver TG levels were determined by enzymatic assay kits (Determiner L, Kyowa Medex, Tokyo, Japan). The concentration of NEFA was measured using NEFA C-test Wako (Wako Pure Chemical, Osaka, Japan). The concentration of total cholesterol was measured using T-cho test Wako (Wako Pure Chemical, Osaka, Japan). Plasma leptin concentration was measured with mouse leptin ELISA kit from Morinaga Institute of Biological Science, Inc. (Kanagawa, Japan).

Histopathology on obesity model mice liver tissues

Portions of liver tissue (from the same lobe at all times) were fixed with Tissue-Tek suffix (Sakura Finetech Japan Co., Ltd., Tokyo, Japan) (18.5% formaldehyde), processed and embedded in paraffin. The tissue was stained with hematoxylin and eosin (H&E) after sectioning.

Oral glucose tolerance test (OGTT)

After 10 weeks of treatment, an oral glucose tolerance test (OGTT) was performed in overnight fasted mice.[79] Glucose was administered by gavage at a dose of 1.5 g/kg body weight. Blood was collected from the tail vein at the indicated time points. Blood glucose concentration was measured with the Life Check (Eisai Co., Ltd., Tokyo, Japan and EIDIA Co., Ltd., Tokyo, Japan). Plasma insulin concentrations were measured with mouse insulin ELISA kit from Morinaga Institute of Biological Science, Inc. (Kanagawa, Japan). GLP-1 in plasma was assayed using the ELISA kit (Immuno-Biological Laboratories Co., Ltd., Gunma, Japan), according to the manufacturer instructions.

Intraperitoneal insulin tolerance test (IPITT)

After 11 weeks of treatment, an intraperitoneal insulin tolerance test (IPITT) was performed in 4 h fasted mice.[80] Insulin (Humulin R U-100, Eli Lilly and Company, IA, USA) was injected at dose of 0.75 U/kg body weight. Blood was collected from the tail vein at the

indicated time points. Blood glucose concentration was measured with the Life Check (Eisai Co., Ltd., Tokyo, Japan and EIDIA Co., Ltd., Tokyo, Japan).

RNA extraction and quantitative RT-PCR

After treatments, blood was collected from the mice for subsequent blood measurements and tissues for RNA isolation. Total RNA was extracted from tissue samples using Rneasy Mini kit (Qiagen, Hilden, Germany). The cDNA was synthesized from total RNA with the PrimeScript RT Master Mix (Takara Bio, Inc., Shiga, Japan). The real-time PCR was performed on the PIKO Real (Thermo Fisher Scientific, MA, USA) using the SYBR Premix Ex TaqII (Takara Bio, Inc., Shiga, Japan). All mRNA expression levels were corrected for expression of the housekeeping gene *18s*. The sequences of the primer sets used are shown in Table S1.

Transcriptome analysis

The transcriptome was measured by Agilent microarray using the SurePrint G3 Mouse GE 8 × 60K Microarray instrument. Data analysis was performed using R software. To assess the reversal of the effects of HFD by nori, we plotted the log2 (fold changes) of the effects of HFD against that of HFD-P and HFD-Ex. The gene set enrichment analyses were performed using the gseGO and gseKEGG functions of the ClusterProfiler package. Plots and heatmaps were generated using the ggplot2 package.

16S rRNA gene sequencing

Fecal samples were collected from respective groups. The total DNA was extracted with the QIAamp PowerFecal Pro DNA Kit (Qiagen, Hilden, Germany) according to the company instructions. For 16S amplicon pyrosequencing, PCR amplification was performed spanning the V4 region using the primers 515F/806R of the 16S rRNA gene and subsequently sequenced using 2 × 250 bp paired-end sequencing (MiSeq, Illumina, Inc., CA, USA) at the BGI, Shenzhen, China. Primer 515F: GTGYCAGCMGCCGCGGTAA; Primer 806R: GGACTACNVGGGTWTCTAA.

Cholesterol composition

Sterol concentrations in liver were measured using our previously described HPLC-ESI-MS/MS method.[81,82] In brief, 5 mg aliquots of liver were incubated with stable isotope-labelled oxysterols as internal standards in 1 N ethanolic KOH at 37°C for 1 h. Sterols were extracted with n-hexane, derivatized to picolinyl esters, and analyzed by HPLC-ESI-MS/MS.

FFA composition

The fatty acid composition of liver was measured by GC-MS/MS using Agilent 7890B 5977 B GC/MSD and GCMS-TQ8030 at the JAPAN TESTING LABORATORIES, Inc. (Gifu, Japan).

Ceramide analysis

Plasma lipids were extracted with chloroform: methanol: water (1: 2: 0.2, v/v/v) solution containing EquiSPLASH (Avanti), fatty acid 18:0 d3 and fatty acid 16:0 d3 as internal standards. Quantification of plasma lipids (ceramides) was performed by liquid chromatography-tandem MS (LC-MS/MS)-based lipidomics as described previously.[83] Lipidomics analyses were performed using an AQUITY UPLC I-class system (Waters Corporation, MA, USA) coupled with TripleTOF 6600 (AB Sciex, Pte. Ltd., MA, USA).

Plasma ALT and AST

ALT and AST levels in plasma were assayed using the enzymatic assay kit (Alanine Aminotransferase Activity Assay Kit, Bio Vision Inc., CA, USA; Aspartate Aminotransferase Activity Colorimetric Assay Kit, Bio Vision Inc., CA, USA), according to the manufacturer instructions.

Histopathology on MASH model mouse liver tissues

Liver tissue samples were fixed in Tissue-Tek suffix (Sakura Finetek Japan Co., Ltd., Tokyo, Japan) (18.5% formaldehyde) for 24 h and then embedded in paraffin. Sirius red and Masson's trichrome stains were used for assessment of hepatic fibrosis. For quantifying the area of fibrosis for Sirius Red staining, images of all fields in each liver sample of the same lobe were processed using ImageJ software (National Institutes of Health, MD, USA).[84]

Bile acid analysis

Samples were heated at 80°C for 20 min in 5% KOH/water, with the addition of internal standards and 0.5 M potassium phosphate buffer (pH 7.4). Bile acids were then extracted using Bond Elut C18 cartridges and quantified by LC-MS/MS. Chromatographic separation utilizes a Hypersil GOLD column with a mobile phase composed of ammonium acetate buffer, acetonitrile, and methanol. The specific gradient program and detailed LC-MS/MS conditions are described elsewhere.[85,86]

Literature review of studies on seaweed waste

MEDLINE was searched for articles published in English from to January 1, 1946 to March 2, 2023. Keywords or phrases for seaweed ("seaweed" or "macroalgae" or "sea vegetables" or "nori"), for waste ("waste" or "by-product" or "discolored" or "food waste" or

"food loss"). Two reviewers (Y.Y. and Tanon T.) independently scanned the retrieved abstracts to identify studies that met the following inclusion criteria: (1) use of seaweed waste, (2) examination of applications using seaweed waste. Exclusion criteria were (1) not an original paper, (2) not an English-language paper, (3) not using seaweed-derived waste.

QUANTIFICATION AND STATISTICAL ANALYSIS

Comparisons between two groups were assessed using Student's t test. Comparisons between more than two groups were assessed using analysis of variance, assessed by Holm-Šídák's multiple comparisons test. We used GraphPad Prism 10 (GraphPad Software, CA, USA) for all other statistical analyses. All p values < 0.05 were considered significant. $^{*}p < 0.05$; $^{**}p < 0.01$; $^{***}p < 0.001$, $^{****}p < 0.0001$ unless stated otherwise. All of the statistical details of experiments can be found in the figure legends.